Neural field modelling

S Coombes

Centre for Mathematical Medicine and Biology,
Department of Mathematical Sciences,
University of Nottingham, Nottingham, NG7 2RD, UK.

email: stephen.coombes@nottingham.ac.uk

November 1, 2011

Abstract

The tools of dynamical systems theory are having an increasing impact on our understanding of patterns of neural activity. In these five lectures I will describe how to build tractable tissue level models that maintain a strong link with biophysical reality. These models typically take the form of nonlinear integro-differential equations. Their non-local nature has led to the development of a set of analytical and numerical tools for the study of spatio-temporal patterns, based around natural extensions of those used for local differential equation models. I present an overview of these techniques, covering Turing instability analysis, amplitude equations, and travelling waves in both homogeneous and heterogeneous models. The last lecture discusses the spiking Lighthouse model of Haken, and advocates this as a tractable model that may allow for the development of an exactly soluble neurodynamics that goes beyond the standard mean field approach.

Lecture 1: Tissue level firing rate models with axo-dendritic connections I

- Turing instability analysis

Lecture 2: Tissue level firing rate models with axo-dendritic connections II

- Amplitude equations
- Brain wave equations

Lecture 3: Travelling waves and localised states

- Construction and stability (Evans functions)
- Interface dynamics

Lecture 4: Waves in random neural media

Lecture 5: Tissue level spiking models: the dynamics of the continuum Lighthouse model

1 Lecture 1

Ever since Hans Berger made the first recording of the human electroencephalogram (EEG) in 1924 there has been a tremendous interest in understanding the physiological basis of brain rhythms. This has included the development of mathematical models of cortical tissue – which are often referred to as neural field models. These have remained pretty much in their current form since the seminal work of Wilson and Cowan [68, 69] and Amari [1, 2] in the 1970s. Here I will develop the discussion of a particular neural field model that incorporates much of the spirit of these original formulations, though with refinements that make a stronger connection to models of both synaptic and dendritic processing.

For a recent review of neural field modelling see [21, 22].

1.1 Synaptic processing

At a synapse presynaptic firing results in the release of neurotransmitters that causes a change in the membrane conductance of the post-synaptic neuron. This post-synaptic current may be written

$$I_s = g(V_s - V), \tag{1}$$

where V is the voltage of the post-synaptic neuron, V_s is the membrane reversal potential and g is a conductance. This is proportional to the probability that a synaptic receptor channel is in an open conducting state. This probability depends on the presence and concentration of neurotransmitter released by the presynaptic neuron. The sign of V_s relative to the resting potential (assumed to be zero) determines whether the synapse is excitatory ($V_s > 0$) or inhibitory ($V_s < 0$).

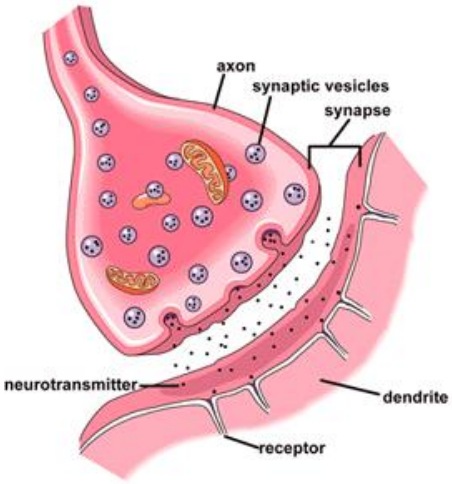

The effect of some synapses can be described with a function that fits the shape of the post-synaptic response due to the arrival of action potential at the pre-synaptic release site. A post-synaptic conductance change $g(t)$ would then be given by

$$g(t) = \overline{g}\eta(t - T), \qquad t \geq T, \tag{2}$$

where T is the arrival time of a pre-synaptic action potential and $\eta(t)$ fits the shape of a realistic post-synaptic conductance. A common (normalised) choice for $\eta(t)$ is a difference of exponentials:

$$\left(\frac{1}{\alpha} - \frac{1}{\beta}\right)^{-1} [\mathrm{e}^{-\alpha t} - \mathrm{e}^{-\beta t}]H(t), \tag{3}$$

or the α-function :

$$\alpha^2 t \mathrm{e}^{-\alpha t} H(t), \tag{4}$$

where H is a Heaviside step function. The conductance change arising from a train of action potentials, with firing times T_m, is given by

$$g(t) = \overline{g} \sum_m \eta(t - T_m). \tag{5}$$

We note that both the forms for $\eta(t)$ above can be written as the Green's function of a linear differential operator, so that $Q\eta = \delta$, where

$$Q = \left(1 + \frac{1}{\alpha}\frac{\mathrm{d}}{\mathrm{d}t}\right)\left(1 + \frac{1}{\beta}\frac{\mathrm{d}}{\mathrm{d}t}\right), \tag{6}$$

for (3) and one simply sets $\beta = \alpha$ to obtain the response describing an α-function.

1.2 Dendritic processing

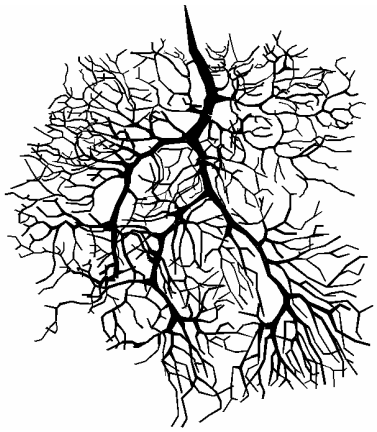

Dendrites form the major components of neurons. They are complex branching structures that receive and process thousands of synaptic inputs from other neurons. It is well known that dendritic morphology plays an important role in the function of dendrites. Another important contribution to the response characteristics of a single neuron comes from the intrinsic resonant properties of dendritic membrane [27]. Visit NeuroMorpho.Org to see a repository of digitally reconstructed neurons. On the right is an example of a digitally reconstructed Purkinje cell.

A nerve fibre consists of a long thin, electrically conducting core surrounded by a thin membrane whose resistance to transmembrane current flow is much greater than that of either the internal core or the surrounding medium. Injected current can travel long distances along the dendritic core before a significant fraction leaks out across the highly resistive cell membrane. Conservation of electric current in an infinitesimal cylindrical element of nerve fibre yields a second–order linear partial differential equation known as the *cable equation*. Let $V(x,t)$ denote the membrane potential at position x along a uniform cable at time t measured relative to the resting potential of the membrane. Let τ be the cell membrane time constant, D the diffusion constant, then the basic uniform (infinite) cable equation is

$$\frac{\partial V(x,t)}{\partial t} = -\frac{V(x,t)}{\tau} + D\frac{\partial^2 V(x,t)}{\partial x^2} + I(x,t), \quad x \in (-\infty, \infty), \tag{7}$$

where we include the source term $I(x,t)$ corresponding to external input injected into the cable. Diffusion along the dendritic tree generates an effective spatio-temporal distribution of delays as expressed by the associated Green's function of the cable equation.

In response to a unit impulse at x' at $t = 0$ and taking $V(x,0) = 0$ the dendritic potential behaves as $V(x,t) = G_\infty(x - x', t)$, where

$$G_\infty(x,t) = \frac{1}{\sqrt{4\pi D t}} \mathrm{e}^{-t/\tau} \mathrm{e}^{-x^2/(4Dt)}. \tag{8}$$

The Green's function $G_\infty(x,t)$determines the linear response to an instantaneous injection of unit current at a given point on the tree. Using the linearity of the cable equation one may write the general solution as

$$V(x,t) = \int_{-\infty}^{t} \mathrm{d}t' \int_{-\infty}^{\infty} \mathrm{d}x' G_\infty(x - x', t - t') I(x', t') + \int_{-\infty}^{\infty} \mathrm{d}x' G_\infty(x - x', t) V(x', 0). \tag{9}$$

For example, assuming the soma is at $x = 0$, $V(x,0) = 0$ and the synaptic input is a train of spikes at $x = x'$, $I(x,t) = \delta(x - x') \sum_m \delta(t - T_m)$ we have that

$$V(0,t) = \sum_m \eta(t - T_m), \qquad \eta(t) = G_\infty(x', t). \tag{10}$$

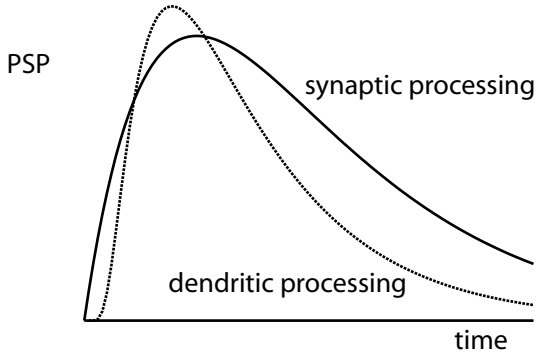

Distributed delays arising from synaptic and dendritic processing have similar shapes.

Green's function for the infinite cable equation

$$G_t = -\frac{G}{\tau} + DG_{xx}, \qquad G(x,0) = \delta(x).$$

Introduce the Fourier transform

$$G(k,t) = \int_{-\infty}^{\infty} \mathrm{e}^{-ikx} G(x,t)\mathrm{d}x, \qquad G(x,t) = \frac{1}{2\pi}\int_{-\infty}^{\infty} \mathrm{e}^{ikx} G(k,t)\mathrm{d}k$$

then

$$G_t(k,t) = -\epsilon(k)G(k,t), \qquad G(k,0) = 1, \quad \epsilon(k) = \frac{1}{\tau} + Dk^2,$$

with solution $G(k,t) = G(k,0)\exp(-\epsilon(k)t)$. Inverse transforming gives

$$\begin{aligned} G(x,t) &= \frac{1}{2\pi}\int_{-\infty}^{\infty} \mathrm{d}k \mathrm{e}^{ikx}\mathrm{e}^{-\epsilon(k)t} = \mathrm{e}^{-t/\tau}\mathrm{e}^{-x^2/4Dt}\frac{1}{2\pi}\int_{-\infty}^{\infty} \mathrm{e}^{-Dt[k+ix/2Dt]^2}\mathrm{d}k \\ &= \frac{1}{\sqrt{4\pi Dt}}\mathrm{e}^{-t/\tau}\mathrm{e}^{-x^2/(4Dt)} \end{aligned}$$

where we complete the square and use the fact that $\int_{-\infty}^{\infty}\exp(-x^2)\mathrm{d}x = \sqrt{\pi}$.

1.3 Tissue level firing rate models with axo-dendritic connections I

At heart modern biophysical theories assert that EEG signals from a single scalp electrode arise from the coordinated activity of $\sim 10^6$ pyramidal cells in cortex [29] (figure on right is from [53]). These are arranged with their dendrites in parallel and perpendicular to the cortical surface. When synchronously activated by synapses at the proximal dendrites extracellular current flows (parallel to the dendrites), with a net membrane current at the synapse. For excitatory (inhibitory) synapses this creates a sink (source) with a negative (positive) extracellular potential. Because there is no accumulation of charge in the tissue the proximal synaptic current is compensated by other currents flowing in the medium causing a distributed source in the case of a sink and vice-versa for a synapse that acts as a source. Hence, at the population level the potential field generated by a synchronously activated population of cortical pyramidal cells behaves like that of a dipole layer. Although the important contribution that single dendritic trees make to generating extracellular electric field potentials has been realised for some time, and can be calculated using Maxwell's equations [57], they are typically not accounted for in neural field models. The exception to this being the work of Bressloff, reviewed in [11].

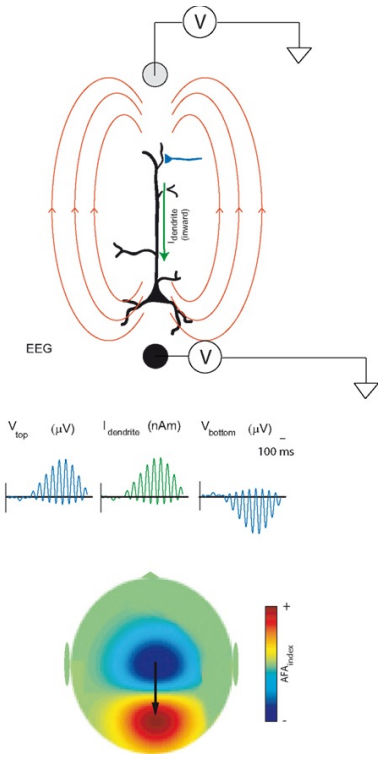

A digression — from spike to rate

In many neural population models it is assumed that the interactons are mediated by firing rates rather than action potentials (spikes) *per se*. To see how this might arise we rewrite (5) in the equivalent form

$$Qg = \overline{g} \sum_m \delta(t - T_m). \tag{11}$$

If we perform a short-time average of (11) over some time-scale Δ and assume that η is sufficiently *slow* so that $\langle Qg \rangle_t$ is approximately constant, where

$$\langle x \rangle_t = \frac{1}{\Delta} \int_{t-\Delta}^{t} x(s) \mathrm{d}s, \tag{12}$$

then we have that $Qg = f$, where f is the instantaneous firing rate (number of spikes per time Δ). For a single neuron (real or synthetic) experiencing a constant drive it is natural to assume that this firing rate is a function of the drive alone. If for the moment we assume that a neuron spends most of its time close to rest such that $V_s - V \approx V_s$, and absorb a factor V_s into g, then for synaptically interacting neurons this drive is directly proportional to the conductance state of the presynaptic neuron. Thus for a single population with self-feedback we are led naturally to equations like:

$$Qg = w_0 f(g), \tag{13}$$

for some strength of coupling w_0. A common choice for the *population* firing rate function is the sigmoid

$$f(g) = \frac{1}{1 + \exp(-\beta(g - h))}, \tag{14}$$

which saturates to one for large g. This functional form, with threshold h and steepness parameter β, is not derived from a biophysical model, rather it is seen as a physiologically consistent choice.

To obtain a tissue level model in one spatial dimension we simply consider $g = g(x,t)$, with $x \in \mathbb{R}$, and introduce a coupling function and integrate over the domain to obtain

$$Qg = \int_{-\infty}^{\infty} w(x,y) f(g(y, t - D(x,y)/v)) \mathrm{d}y. \quad (15)$$

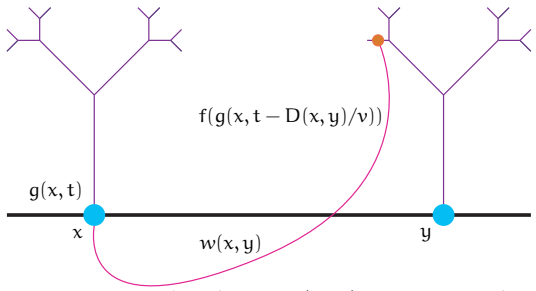

Here we have allowed for a communication delay, that arises because of the finite speed, v, of the action potential, where $D(x,y)$ measures the length of the axonal fibre between points at x and y. The coupling function $w(x,y)$ represents anatomical connectivity, and is often assumed to be homogeneous so that $w(x,y) = w(|x-y|)$. It is also common to assume that $D(x,y) = |x-y|$. With these assumptions and for the special case $v \to \infty$, $Q = (1 + \mathrm{d}/\mathrm{d}t)$, we recover the standard Amari model. Extending the above ideas to populations of excitatory and inhibitory conductances allows one to recover the related Wilson-Cowan model. □

Following the original work of Bressloff (reviewed in [11]) we now develop the cable modelling approach of Rall [62] to describe a firing rate cortical tissue model with axo-dendritic patterns of synaptic connectivity. For simplicity we shall consider only an effective single population model in one (somatic) spatial dimension to include a further dimension representing position along a (semi-infinite) dendritic cable. The firing rate in the somatic (cell body) layer is taken to be a smooth function of the cable voltage at the soma, which is in turn determined by the spatio-temporal pattern of synaptic currents on the cable. The extension to two-dimensional layers and mixtures of excitatory and inhibitory synapses across the model of a branched dendritic tree is still a research direction worthy of further investigation.

The voltage $V(\xi, x, t)$ at position $\xi \geq 0$ along a semi-infinite passive cable with somatic coordinate $x \in \mathbb{R}$ can then be written:

$$\frac{\partial V}{\partial t} = -\frac{V}{\tau} + D\frac{\partial^2 V}{\partial \xi^2} + I(\xi, x, t). \quad (16)$$

Here, $I(\xi, x, t)$ is the synaptic input, and we shall drop shunting effects and take this to be directly proportional to a conductance change, which evolves according to the usual neural field prescription (see above) as

$$g(\xi, x, t) = \int_{-\infty}^{t} \mathrm{d}s \eta(t-s) \int_{-\infty}^{\infty} \mathrm{d}y W(\xi, x, y) f(h(y, s - D(x,y)/v)). \quad (17)$$

The function $W(\xi, x, y)$ describes the axo-dendritic connectivity pattern and the field h is taken as a measure of the drive at the soma. As a simple model of h we shall take it to be the somatic potential and write $h(x,t) = V(0, x, t)$. For no flux boundary conditions $\partial V(\xi, x, t)/\partial \xi|_{\xi=0} = 0$, and assuming vanishing initial data, we may write the solution to (16) in the form

$$V(\xi, x, t) = \kappa (G \otimes g)(\xi, x, t), \quad G = 2G_\infty \quad (18)$$

for some constant of proportionality $\kappa > 0$, where $G_\infty(x,t)$ is given by (8) and the operator $\otimes$ denotes spatio-temporal convolution over the (ξ, t) coordinates. Further assuming that the axo-dendritic weights can be decomposed in the product form $W(\xi, x, y) = P(\xi) w(|x-y|)$ then the equation for h takes the form

$$h(x,t) = \kappa \int_{-\infty}^{t} \mathrm{d}s F(t-s) \int_{-\infty}^{s} \mathrm{d}s' \eta(s-s') \int_{-\infty}^{\infty} \mathrm{d}y w(|x-y|) f(h(y, s' - D(x,y)/v)), \quad (19)$$

where

$$F(t) = \int_0^\infty \mathrm{d}\xi P(\xi) G(\xi, t). \tag{20}$$

1.4 Turing instability analysis

To assess the pattern forming properties of the model it is useful to perform a Turing instability analysis. This describes how a spatially homogeneous state can become unstable to spatially heterogeneous perturbations, resulting in the formation of periodic patterns. To illustrate the technique consider the one-dimensional model without dendrites or axonal delays, obtained in the limit $v \to \infty$ and $F(t) \to \delta(t)$:

$$h(x,t) = \kappa \int_0^\infty \mathrm{d}s \eta(s) \int_{-\infty}^\infty \mathrm{d}y w(|y|) f(h(x-y, t-s)). \tag{21}$$

One solution of the neural field equation is the spatially uniform resting state $h(x,t) = h_0$ for all x, t, defined by

$$h_0 = \kappa f(h_0) \int_{-\infty}^\infty w(|y|) \mathrm{d}y. \tag{22}$$

Here we have used the fact that η is normalised, namely that $\int_0^\infty \mathrm{d}s \eta(s) = 1$. We linearise about this state by letting $h(x,t) \to h_0 + h(x,t)$ so that $f(h) \to f(h_0) + f'(h_0)u$ to obtain

$$h(x,t) = \kappa\beta \int_0^\infty \mathrm{d}s \eta(s) \int_{-\infty}^\infty \mathrm{d}y w(y) h(x-y, t-s), \qquad \beta = f'(h_0). \tag{23}$$

This has solutions of the form $\mathrm{e}^{\lambda t}\mathrm{e}^{ipx}$, with a dispersion curve:

$$1 = \kappa\beta \widetilde{\eta}(\lambda) \widehat{w}(p), \qquad \widehat{w}(p) = \int_{-\infty}^\infty \mathrm{d}y w(|y|) \mathrm{e}^{-ipy}, \qquad \widetilde{\eta}(\lambda) = \int_0^\infty \mathrm{d}s \eta(s) \mathrm{e}^{-\lambda s}. \tag{24}$$

We recognise $\widehat{w}$ as the Fourier transform of w and $\widetilde{\eta}$ as the Laplace transform of η. The uniform steady state is linearly stable if $\mathrm{Re}\lambda(p) < 0$ for all $p \in \mathbb{R}$, $p \neq 0$. For the choice $\eta(t) = \alpha \mathrm{e}^{-\alpha t} H(t)$ (so that $Q = (1 + \alpha^{-1}\mathrm{d}/\mathrm{d}t)$) then $\widetilde{\eta}(\lambda) = (1 + \lambda/\alpha)^{-1}$. In this case, since $w(x) = w(-x)$ then $\widehat{w}(p)$ is a real even function of p and the stability condition is simply

$$\widehat{w}(p) < \frac{1}{\beta\kappa}, \qquad \text{for all } \; p \in \mathbb{R}, \quad p \neq 0. \tag{25}$$

Now consider the case that $\widehat{w}(p)$ has a positive maximum $\widehat{w}_{\max}$ at $p = \pm p_c$, that is $\widehat{w}(p_c) = \widehat{w}_{\max}$ and $\widehat{w}(p) < \widehat{w}_{\max}$ for all $p \neq p_c$. Let

$$\beta_c = \frac{1}{\kappa \widehat{w}_{\max}} \tag{26}$$

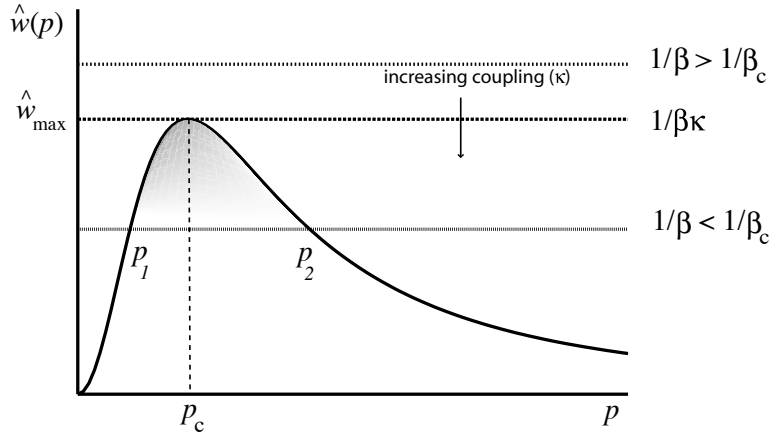

- For $\beta < \beta_c$ we have $\kappa\widehat{w}(p) \leq \kappa\widehat{w}_{\max} < 1/\beta$ for all p and the resting state is linearly stable.
- At the critical point $\beta = \beta_c$ we have $\beta_c\kappa\widehat{w}(p_c) = 1$ and $\beta_c\kappa\widehat{w}(p) < 1$ for all $p \neq p_c$. Hence, $\lambda(p) < 0$ for all $p \neq p_c$, but $\lambda(p_c) = 0$. This signals the point of a *static* instability due to excitation of the pattern $\mathrm{e}^{\pm ip_c x}$.
- Beyond the bifurcation point, $\beta > \beta_c$, $\lambda(p_c) > 0$ and this pattern grows with time. In fact there will typically exist a range of values of $p \in (p_1, p_2)$ for which $\lambda(p) > 0$, signalling a set of growing patterns. As the patterns grow, the linear approximation breaks down and nonlinear terms dominate behaviour.
- The saturating property of $f(u)$ tends to create patterns with finite amplitude, that scale as $\sqrt{\beta - \beta_c}$ close to bifurcation and have wavelength $2\pi/p_c$.
- If $p_c = 0$ then we would have a *bulk instability* resulting in the formation of another homogeneous state.

A biologically motivated choice for $w(x)$ is the so-called mexican hat function which represents short-range excitation and long-range inhibition. An example of such a function is a difference of two exponentials:

$$w(x) = \Lambda\left[\mathrm{e}^{-\gamma_1|x|} - \Gamma\mathrm{e}^{-\gamma_2|x|}\right], \tag{27}$$

with $\Gamma < 1$, $\gamma_1 > \gamma_2 > 0$ and $\Lambda = +1$. (The case $\Lambda = -1$, which represents short-range inhibition and long-range excitation will be considered below in the full model). The Fourier transform $\widehat{w}(p)$ is calculated as:

$$\widehat{w}(p) = 2\Lambda\left[\frac{\gamma_1}{\gamma_1^2 + p^2} - \Gamma\frac{\gamma_2}{\gamma_2^2 + p^2}\right], \tag{28}$$

from which we may determine p_c as

$$p_c^2 = \frac{\gamma_1^2\sqrt{\Gamma\gamma_2/\gamma_1} - \gamma_2^2}{1 - \sqrt{\Gamma\gamma_2/\gamma_1}}. \tag{29}$$

Hence, $p_c \neq 0$ when $\Gamma > (\gamma_2/\gamma_1)^3$. Note that for $\Lambda = -1$ then $p_c = 0$ and a Turing instability does not occur.

For the full model (19) with $D(x, y) = |x - y|$ the homogeneous steady state, $h(x, t) = h_0$ for all x, t, satisfies

$$h_0 = \kappa f(h_0)\int_0^\infty F(s)\mathrm{d}s\int_{-\infty}^\infty \mathrm{d}y w(|y|), \tag{30}$$

and the spectral equation takes the form

$$1 = \kappa\beta\widehat{w}(p, \lambda)\widetilde{\eta}(\lambda)\widetilde{F}(\lambda), \qquad \widehat{w}(p, \lambda) = \int_{-\infty}^\infty \mathrm{d}y w(|y|)\mathrm{e}^{-ipy}\mathrm{e}^{-\lambda|y|/v}, \qquad \beta = f'(h_0). \tag{31}$$

Compared to (24) it is now possible for complex solutions for λ to be supported – allowing for the possibility of *dynamic* (as opposed to static) Turing instabilities to occur. These occur when $\mathrm{Im}\,\lambda \neq 0$ at the bifurcation point.

For example, in the limit $v \to \infty$ then $\widehat{w}(p, \lambda) \to \widehat{w}(p)$ and for $\eta(t) = \alpha\mathrm{e}^{-\alpha t}H(t)$ we have that

$$1 + \lambda/\alpha = \kappa\beta\widehat{w}(p)\widetilde{F}(\lambda). \tag{32}$$

A necessary condition for a dynamic instability ($\mathrm{Re}\,\lambda = 0$ and $\mathrm{Im}\,\lambda \neq 0$) is that there exists a pair ω, $p \neq 0$ such that

$$1 + i\omega/\alpha = \kappa\beta\widehat{w}(p)\widetilde{F}(i\omega). \tag{33}$$

Equating real and imaginary parts (and using the fact that $\widehat{w}(p) \in \mathbb{R}$) gives us the pair of simultaneous equations

$$1 = \kappa\beta\widehat{w}(p)C(\omega), \qquad \omega/\alpha = \kappa\beta\widehat{w}(p)S(\omega), \tag{34}$$

where $C(\omega) = \mathrm{Re}\,\widetilde{F}(i\omega)$ and $S(\omega) = \mathrm{Im}\,\widetilde{F}(i\omega)$. Note that $C(\omega) = \int_0^\infty \mathrm{d}s F(s)\cos(\omega s) \leq |C(0)|$. Hence (dividing the above equations) if there is a non-zero solution to

$$\frac{\omega_c}{\alpha} = \mathcal{H}(\omega_c), \qquad \mathcal{H}(\omega_c) \equiv \frac{S(\omega_c)}{C(\omega_c)}, \tag{35}$$

then the bifurcation condition, $\beta = \beta_d$, for a dynamic instability is defined by

$$\beta_d \kappa \widehat{w}(p_{\text{min}}) = \frac{1}{C(\omega_c)}, \tag{36}$$

which should be contrasted with the bifurcation condition, $\beta = \beta_s$, for a static instability, namely

$$\beta_s \kappa \widehat{w}(p_{\text{max}}) = \frac{1}{C(0)}, \tag{37}$$

where

$$\widehat{w}(p_{\text{min}}) = \min_p \widehat{w}(p), \qquad \widehat{w}(p_{\text{max}}) = \max_p \widehat{w}(p). \tag{38}$$

Assuming that $\widehat{w}(p_{\text{min}}) < 0 < \widehat{w}(p_{\text{max}})$, a dynamic Turing instability will occur if $\beta < \beta_s$ and $p_{\text{min}} \neq 0$, whereas a static Turing instability will occur if $\beta_s < \beta$ and $p_{\text{max}} \neq 0$.

For the Mexican hat function (27) with $\Lambda = +1$ (short-range excitation, long-range inhibition), a dynamic Turing instability is not possible since $p_{\text{min}} = 0$. However, it is possible for bulk oscillations to occur instead of static patterns when

$$\widehat{w}(p_c) < -\frac{C(\omega_c)}{C(0)}|\widehat{w}(0)|, \tag{39}$$

with p_c given by (29). On the other hand, when $\Lambda = -1$ (short-range inhibition, long-range excitation) a dynamic instability can occur since $p_{\text{min}} = p_c$ and $p_{\text{max}} = 0$, provided that

$$\widehat{w}(0) < -\frac{C(\omega_c)}{C(0)}|\widehat{w}(p_c)|. \tag{40}$$

As an explicit example consider the choice $P(\xi) = \delta(\xi - \xi_0)$ (so that the synaptic contact occurs at a fixed distance from the dendrite). In this case $F(t) = G(\xi_0, t)$ with Laplace transform:

$$\widetilde{F}(\lambda) = \frac{\mathrm{e}^{-\gamma(\lambda)\xi_0}}{D\gamma(\lambda)}, \qquad \gamma^2(\lambda) = (1/\tau + \lambda)/D. \tag{41}$$

In this case we may calculate the real and imaginary parts of $\widetilde{F}(i\omega)$ as

$$C(\omega) = \frac{1}{\sqrt{1/\tau^2 + \omega^2}}\mathrm{e}^{-A(\omega)\xi_0}[A(\omega)\cos(B(\omega)\xi_0) - B(\omega)\sin(B(\omega)\xi_0)] \tag{42}$$

$$S(\omega) = -\frac{1}{\sqrt{1/\tau^2 + \omega^2}}\mathrm{e}^{-A(\omega)\xi_0}[A(\omega)\sin(B(\omega)\xi_0) + B(\omega)\cos(B(\omega)\xi_0)], \tag{43}$$

where $\sqrt{(1/\tau + i\omega)/D} = A(\omega) + iB(\omega)$ so that

$$A(\omega) = \sqrt{[\sqrt{1/(\tau D)^2 + \omega^2/D^2} + 1/(\tau D)]/2}, \qquad B(\omega) = \sqrt{[\sqrt{1/(\tau D)^2 + \omega^2/D^2} - 1/(\tau D)]/2}. \tag{44}$$

A plot of $H(\omega)$ is shown in Fig. 1, highlighting the possibility of a non-zero solution of (35) for a certain parameter set (and hence the possibility of a dynamic instability).

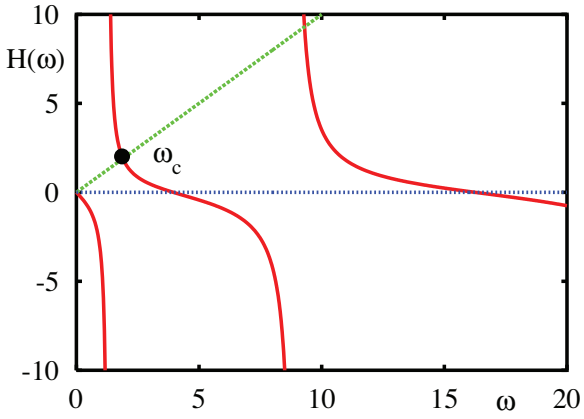

Figure 1: A plot of the function $H(\omega)$ for $D = \tau = 1$ with $\xi_0 = 2$, showing a non-zero solution of (35) for $\alpha = 1$.

Laplace transform of $G_\infty(\xi, t)$

$$G_t = -\frac{G}{\tau} + DG_{\xi\xi}, \qquad G(\xi, 0) = \delta(\xi).$$

Introduce the Laplace transform

$$G(\xi, \lambda) = \int_0^\infty \mathrm{d}s \mathrm{e}^{-\lambda s} G(\xi, s), \qquad \gamma^2(\lambda) = (1/\tau + \lambda)/D.$$

then

$$\left[\gamma^2(\lambda) - \mathrm{d}_{\xi\xi}\right] G(\xi, \lambda) = \delta(\xi)/D.$$

This second order ODE has the solution

$$G(\xi, \lambda) = \frac{\mathrm{e}^{-\gamma(\lambda)\xi}}{2D\gamma(\lambda)}.$$

For a discussion of dynamic Turing instabilities with finite v we refer the reader to [67]. For the treatment of more general forms of axo-dendritic connectivity (that do not assume a product form) we refer the reader to [8, 14].

A generalisation of our argument to two dimensions shows that the linearised equations of motion have solutions of the form $e^{\lambda t}e^{i\mathbf{p}\cdot\mathbf{r}}$, $\mathbf{r},\mathbf{p}\in\mathbb{R}^2$, with $\lambda=\lambda(p)$, $p=|\mathbf{p}|$ as determined by (31) with

$$\widehat{w}(p,\lambda)=\int_{\mathbb{R}^2}\mathrm{d}\mathbf{r}w(|\mathbf{r}|)e^{-i\mathbf{p}\cdot\mathbf{r}}e^{-\lambda|\mathbf{r}|/v}. \quad (45)$$

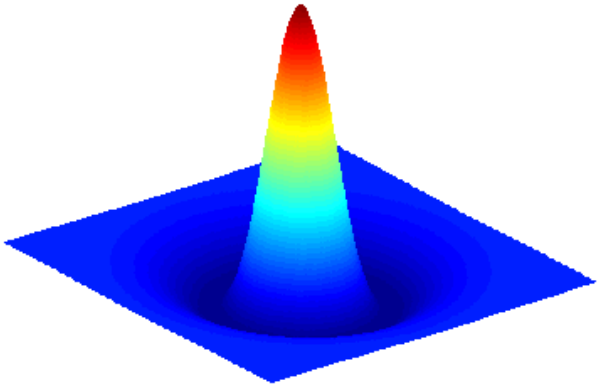

Near bifurcation we expect spatially periodic solutions of the form $\exp i[p_1x+p_2y]$, $p_c^2=p_1^2+p_2^2$. For a given p_c there are an infinite number of choices for p_1 and p_2. It is therefore convenient to restrict attention to doubly periodic solutions that tessellate the plane. These can be expressed in terms of the basic symmetry groups of hexagon, square and rhombus. Solutions can then be constructed from combinations of the basic functions $e^{ip_c\mathbf{R}\cdot\mathbf{r}}$, for appropriate choices of the basis vectors $\mathbf{R}$. If ϕ is the angle between two basis vectors $\mathbf{R}_1$ and $\mathbf{R}_2$, we can distinguish three types of lattice according to the value of ϕ: square lattice ($\phi=\pi/2$), rhombic lattice ($0<\phi<\pi/2$) and hexagonal ($\phi=\pi/3$). Hence, all doubly periodic functions may be written as a linear combination of plane waves

$$h(\mathbf{r})=\sum_j A_j e^{ip_c\mathbf{R}_j\cdot\mathbf{r}}+\mathrm{cc}, \qquad |\mathbf{R}_j|=1. \quad (46)$$

For hexagonal lattices we use

$$\mathbf{R}_1=\begin{bmatrix}1\\0\end{bmatrix}, \qquad \mathbf{R}_2=\frac{1}{2}\begin{bmatrix}-1\\\sqrt{3}\end{bmatrix}, \qquad \mathbf{R}_3=\frac{1}{2}\begin{bmatrix}1\\\sqrt{3}\end{bmatrix}. \quad (47)$$

For square lattices we use

$$\mathbf{R}_1=\begin{bmatrix}1\\0\end{bmatrix}, \qquad \mathbf{R}_2=\begin{bmatrix}0\\1\end{bmatrix}, \quad (48)$$

while the rhombus tessellation uses

$$\mathbf{R}_1=\begin{bmatrix}1\\0\end{bmatrix}, \qquad \mathbf{R}_2=\begin{bmatrix}\cos\eta\\\sin\eta\end{bmatrix}. \quad (49)$$

For applications to geometric visual hallucinations see [32, 13].

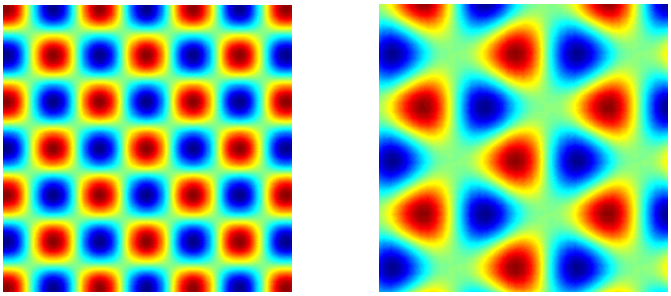

Density plot of doubly periodic square and hexagonal functions.

2 Lecture 2

2.1 Tissue level firing rate models with axo-dendritic connections II

A characteristic feature of the dynamics of systems beyond an instability is the slow growth of the dominant eigenmode, giving rise to the notion of a *separation of scales*. This observation is key in deriving the so-called *amplitude equations*. In this approach information about the short-term behaviour of the system is discarded in favour of a description on some appropriately identified slow time-scale. By Taylor-expansion of the dispersion curve near its maximum one expects the scalings $\mathrm{Re}\,\lambda \sim \beta - \beta_c,\ p - p_c \sim \sqrt{\beta - \beta_c}$, close to bifurcation, where β is the bifurcation parameter. Since the eigenvectors at the point of instability are of the type $A_1 \mathrm{e}^{i(\omega_c t + p_c x)} + A_2 \mathrm{e}^{i(\omega_c t - p_c x)} + \mathrm{cc}$, for $\beta > \beta_c$ emergent patterns are described by an infinite sum of unstable modes (in a continuous band) of the form $\mathrm{e}^{\nu_0(\beta-\beta_c)t}\mathrm{e}^{i(\omega_c t + p_c x)}\mathrm{e}^{ip_0\sqrt{\beta-\beta_c}x}$. Let us denote $\beta = \beta_c + \epsilon^2\delta$ where ϵ is arbitrary and δ is a measure of the distance from the bifurcation point. Then, for small ϵ we can separate the dynamics into fast eigen-oscillations $\mathrm{e}^{i(\omega_c t + p_c x)}$, and slow modulations of the form $\mathrm{e}^{\nu_0\epsilon^2 t}\mathrm{e}^{ip_0\epsilon x}$. If we set as further independent variables $\tau = \epsilon^2 t$ for the modulation time-scale and $\chi = \epsilon x$ for the long-wavelength spatial scale (at which the interactions between excited nearby modes become important) we may write the weakly nonlinear solution as $A_1(\chi,\tau)\mathrm{e}^{i(\omega_c t + p_c x)} + A_2(\chi,\tau)\mathrm{e}^{i(\omega_c t - p_c x)} + \mathrm{cc}$. It is known from the standard theory [43] that weakly nonlinear solutions will exist in the form of either travelling waves ($A_1 = 0$ or $A_2 = 0$) or standing waves ($A_1 = A_2$).

2.2 Amplitude equations

We are now in a position to derive the envelope or *amplitude equations* for patterns emerging beyond the point of an instability for a neural field model. These are also useful for determining the sub- or super-critical nature of the bifurcation. For clarity we shall first focus on the case of a static instability, and consider the example system given by (15) with $\eta(t) = \mathrm{e}^{-t}H(t)$ and $v \to \infty$. In this case the model is conveniently written as an integro-differential equation:

$$\frac{\partial g}{\partial t} = -g + w \otimes f(g), \tag{50}$$

where the symbol $\otimes$ denotes spatial convolution (assuming $w(x,y) = w(|x-y|)$).

We first Taylor expand the nonlinear firing rate around the steady state g_0:

$$f(g) = f(g_0) + \beta_1(g-g_0) + \beta_2(g-g_0)^2 + \beta_3(g-g_0)^3 + \ldots, \tag{51}$$

where $\beta_1 = f'(g_0)$, $\beta_2 = f''(g_0)/2$ and $\beta_3 = f'''(g_0)/6$. We also adopt the perturbation expansion

$$g = g_0 + \epsilon g_1 + \epsilon^2 g_2 + \epsilon^3 g_3 + \ldots\ . \tag{52}$$

After rescaling time according to $\tau = \epsilon^2 t$ and setting $\beta_1 = \beta_c + \epsilon^2\delta$, where β_c is defined by the bifurcation condition $\beta_c = 1/\widehat{w}_{\mathrm{max}}$, we then substitute into (50). Equating powers of ϵ leads to a hierarchy of equations:

$$g_0 = f(g_0)\int_{-\infty}^{\infty} w(|y|)\mathrm{d}y, \tag{53}$$

$$0 = \mathcal{L}g_1, \tag{54}$$

$$0 = \mathcal{L}g_2 + \beta_2 w \otimes g_1^2, \tag{55}$$

$$\frac{\mathrm{d}g_1}{\mathrm{d}\tau} = \mathcal{L}g_3 + \delta w \otimes g_1 + 2\beta_2 w \otimes g_1 g_2 + \beta_3 w \otimes g_1^3, \tag{56}$$

where

$$\mathcal{L}g = -g + \beta_c w \otimes g. \tag{57}$$

The first equation fixes the steady state g_0. The second equation is linear with solutions $g_1 = A(\tau)\mathrm{e}^{ip_c x} + \mathrm{cc}$ (where p_c is the critical wavenumber at the static bifurcation). Hence the null space of $\mathcal{L}$ is spanned by $\mathrm{e}^{\pm ip_c x}$. A dynamical equation for the complex amplitude $A(\tau)$ (and we do not treat here any slow spatial variation) can be obtained by deriving solvability conditions for the higher-order equations, a method known as the Fredholm alternative. These equations have the general form $\mathcal{L}g_n = v_n(g_0, g_1, \ldots, g_{n-1})$ (with $\mathcal{L}g_1 = 0$). We define the inner product of two periodic functions (with periodicity $2\pi/p_c$) as

$$\langle U, V\rangle = \frac{p_c}{2\pi}\int_0^{2\pi/p_c} U^*(x)V(x)\mathrm{d}x, \tag{58}$$

where * denotes complex conjugation. It is simple to show that $\mathcal{L}$ is self-adjoint with respect to this inner product, so that

$$\langle g_1, \mathcal{L}g_n\rangle = \langle \mathcal{L}g_1, g_n\rangle = 0. \tag{59}$$

Hence we obtain the set of solvability conditions

$$\langle \mathrm{e}^{\pm ip_c x}, v_n\rangle = 0, \qquad n \geq 2. \tag{60}$$

The solvability condition with $n = 2$ is automatically satisfied, since $w \otimes g_1^2 = \widehat{w}(2p_c)[A^2\mathrm{e}^{2ip_c x} + \mathrm{cc}] + 2|A|^2\widehat{w}(0)$, and we make use of the result $\langle \mathrm{e}^{imp_c x}, \mathrm{e}^{inp_c x}\rangle = \delta_{m,n}$. For $n = 3$ the solvability condition (projecting onto $\mathrm{e}^{+ip_c x}$) is

$$\langle \mathrm{e}^{ip_c x}, \frac{\mathrm{d}g_1}{\mathrm{d}\tau} - \delta w \otimes g_1\rangle = \beta_3\langle \mathrm{e}^{ip_c x}, w \otimes g_1^3\rangle + 2\beta_2\langle \mathrm{e}^{ip_c x}, w \otimes g_1 g_2\rangle. \tag{61}$$

The left-hand side is easily calculated, using $w \otimes g_1 = \widehat{w}(p_c)[A\mathrm{e}^{ip_c x} + \mathrm{cc}]$, as

$$\frac{\mathrm{d}A}{\mathrm{d}\tau} - \delta\widehat{w}(p_c)A = \frac{\mathrm{d}A}{\mathrm{d}\tau} - \beta_c^{-1}\delta A, \tag{62}$$

where we have made use of the bifurcation condition $\beta_c = 1/\widehat{w}(p_c)$. To evaluate the right-hand side we use the result that $w \otimes g_1^3 = \widehat{w}(p_c)[A^3\mathrm{e}^{i3p_c x} + \mathrm{cc}] + 3|A|^2\widehat{w}(p_c)[A\mathrm{e}^{ip_c x} + \mathrm{cc}]$, to obtain

$$\langle \mathrm{e}^{ip_c x}, w \otimes g_1^3\rangle = 3\beta_c^{-1}A|A|^2. \tag{63}$$

The next step is to determine g_2. From (55) we have that

$$-g_2 + \beta_c w \otimes g_2 = -\beta_2\left\{\widehat{w}(2p_c)[A^2\mathrm{e}^{2ip_c x} + \mathrm{cc}] + 2|A|^2\widehat{w}(0)\right\}. \tag{64}$$

We now set

$$g_2 = A_+\mathrm{e}^{2ip_c x} + A_-\mathrm{e}^{-2ip_c x} + A_0 + \phi g_1. \tag{65}$$

The constant ϕ remains undetermined at this order of perturbation but does not appear in the amplitude equation for $A(\tau)$. Substitution into (64) and equating powers of $\mathrm{e}^{ip_c x}$ gives

$$A_0 = \frac{2\beta_2|A|^2\widehat{w}(0)}{1 - \beta_c\widehat{w}(0)}, \quad A_+ = \frac{\beta_2 A^2\widehat{w}(2p_c)}{1 - \beta_c\widehat{w}(2p_c)}, \quad A_- = A_+^*, \tag{66}$$

where we have used the result that $w \otimes g_2 = \widehat{w}(2p_c)[A_+\mathrm{e}^{2ip_c x} + A_-\mathrm{e}^{-2ip_c x}] + \widehat{w}(0)A_0 + \phi[A\widehat{w}(p_c)\mathrm{e}^{ip_c x} + \mathrm{cc}]$. We then find that

$$\langle \mathrm{e}^{ip_c x}, w \otimes g_1 g_2\rangle = \widehat{w}(p_c)[A_+A^* + A_0 A]. \tag{67}$$

Combining (62), (63) and (67) we obtain the Stuart-Landau equation

$$\beta_c \frac{\mathrm{d}A}{\mathrm{d}\tau} = A(\delta - \Phi|A|^2), \tag{68}$$

where

$$\Phi = -3\beta_3 - 2\beta_2^2 \left[\frac{\widehat{w}(2p_c)}{1-\beta_c\widehat{w}(2p_c)} + \frac{2\widehat{w}(0)}{1-\beta_c\widehat{w}(0)} \right]. \tag{69}$$

Introducing $A = R\mathrm{e}^{i\theta}$ we may rewrite equation (68) as

$$\beta_c \frac{\mathrm{d}R}{\mathrm{d}\tau} = \delta R - \Phi R^3, \qquad \frac{\mathrm{d}\theta}{\mathrm{d}\tau} = 0. \tag{70}$$

Hence, the phase of A is arbitrary ($\theta = \text{const}$) and the amplitude has a pitchfork bifurcation which is super-critical for $\Phi > 0$ and sub-critical for $\Phi < 0$.

Amplitude equations arising for systems with a dynamic instability are treated in [67]. The appropriate amplitude equations are found to be the coupled mean-field Ginzburg–Landau equations describing a Turing–Hopf bifurcation with modulation group velocity of $O(1)$.

In two spatial dimensions the same ideas go across and can be used to determine the selection of patterns (say stripes vs. spots) [30]. In the hierarchy of equations (53) to (56) the symbol $\otimes$ now represents a convolution in two spatial dimensions. The two dimensional Fourier transform $\widehat{w}$ takes the explicit form

$$\widehat{w}(p_1, p_2) = \int_{-\infty}^{\infty} \mathrm{d}x \int_{-\infty}^{\infty} \mathrm{d}y w(x,y) \mathrm{e}^{i(p_1 x + p_2 y)}, \tag{71}$$

and the inner product for periodic scalar functions defined on the plane is defined by

$$\langle U, V \rangle = \frac{1}{|\Omega|} \int_{\Omega} U^*(\mathbf{r}) V(\mathbf{r}) \mathrm{d}\mathbf{r}, \tag{72}$$

with $\Omega = (0, 2\pi/p_c) \times (0, 2\pi/p_c)$. We shall assume a radially symmetric kernel so that $\widehat{w}(p_1, p_2) = \widehat{w}(\sqrt{p_1^2 + p_2^2})$. One composite pattern that solves the linearised equations is

$$g_1(x, y, \tau) = A_1(\tau)\mathrm{e}^{ip_c x} + A_2(\tau)\mathrm{e}^{ip_c y} + \text{cc}. \tag{73}$$

For $A_1 = 0$ and $A_2 \neq 0$ we have a *stripe*, while if both A_1 and A_2 are non-zero, and in particular equal, we have a *spot*. Here p_c is defined by the condition $\beta_c = 1/\widehat{w}(p_c)$. The null space of $\mathcal{L}$ is spanned by $\{\mathrm{e}^{\pm ip_c x}, \mathrm{e}^{\pm ip_c y}\}$, and we may proceed as for the one dimensional case to generate a set of coupled equations for the amplitudes A_1 and A_2. It is simple to show that

$$\langle \mathrm{e}^{ip_c x}, w \otimes g_1^3 \rangle = 3\beta_c^{-1} A_1(|A_1|^2 + 2|A_2|^2). \tag{74}$$

Assuming a representation for g_2 as

$$\begin{aligned} g_2 = {} & \alpha_0 + \alpha_1 \mathrm{e}^{2ip_c x} + \alpha_2 \mathrm{e}^{-2ip_c x} + \alpha_3 \mathrm{e}^{2ip_c y} + \alpha_4 \mathrm{e}^{-2ip_c y} + \alpha_5 \mathrm{e}^{ip_c(x+y)} \\ & + \alpha_6 \mathrm{e}^{-ip_c(x+y)} + \alpha_7 \mathrm{e}^{ip_c(x-y)} + \alpha_8 \mathrm{e}^{-ip_c(x-y)} + \phi g_1, \end{aligned} \tag{75}$$

allows us to calculate

$$\langle \mathrm{e}^{ip_c x}, w \otimes g_1 g_2 \rangle = \beta_c^{-1}[\alpha_0 A_1 + \alpha_1 A_1^* + \alpha_5 A_2^* + \alpha_7 A_2]. \tag{76}$$

Balancing terms in (55) gives

$$\alpha_0 = \frac{2\beta_2(|A_1|^2 + |A_2|^2)\widehat{w}(0)}{1-\beta_c\widehat{w}(0)}, \quad \alpha_1 = \frac{\beta_2 A_1^2 \widehat{w}(2p_c)}{1-\beta_c\widehat{w}(2p_c)}, \quad \alpha_5 = \frac{2\beta_2 A_1 A_2 \widehat{w}(\sqrt{2}p_c)}{1-\beta_c\widehat{w}(\sqrt{2}p_c)}, \quad \alpha_7 = \frac{2\beta_2 A_1 A_2^* \widehat{w}(\sqrt{2}p_c)}{1-\beta_c\widehat{w}(\sqrt{2}p_c)}. \tag{77}$$

Combining the above yields the coupled amplitude equations:

$$\beta_c \frac{\mathrm{d}A_1}{\mathrm{d}\tau} = A_1(\delta - \Phi|A_1|^2 - \Psi|A_2|^2), \qquad \beta_c \frac{\mathrm{d}A_2}{\mathrm{d}\tau} = A_2(\delta - \Phi|A_2|^2 - \Psi|A_1|^2), \tag{78}$$

where

$$\Phi = -3\beta_3 - 2\beta_2^2\left[\frac{2\widehat{w}(0)}{1-\beta_c\widehat{w}(0)} + \frac{\widehat{w}(2p_c)}{1-\beta_c\widehat{w}(2p_c)}\right], \qquad \Psi = -6\beta_3 - 4\beta_2^2\left[\frac{\widehat{w}(0)}{1-\beta_c\widehat{w}(0)} + \frac{2\widehat{w}(\sqrt{2}p_c)}{1-\beta_c\widehat{w}(\sqrt{2}p_c)}\right]. \tag{79}$$

Stripes: The solution $A_2 = 0$, $|A_1| = \sqrt{\delta/\Phi}$ (or vice versa) is stable if and only if $\Psi > \Phi > 0$.
Spots: The solution $|A_1| = |A_2| = \sqrt{\delta/(\Phi+\Psi)}$ is stable if and only if $\Phi > \Psi > 0$.
Hence, stripes and spots are mutually exclusive as stable patterns. In the absence of quadratic terms in f, namely $\beta_2 = 0$, then $\Psi = -6\beta_3$ and $\Phi = -3\beta_3$ so that for an odd firing rate function like $f(x) = \tanh x \simeq x - x^3/3$ then $\beta_3 < 0$ and so $\Psi > \Phi$ and stripes are selected over spots. The key to the appearance of spots is non-zero quadratic terms, $\beta_2 \neq 0$, in the firing rate function; without these terms spots can never stably exist. For a Mexican hat connectivity then $\widehat{w}(\sqrt{2}p_c) > \widehat{w}(2p_c)$ and the quadratic term of Ψ is larger than that of Φ so that as $|\beta_2|$ increases then spots will arise instead of stripes.

The technique above can also be used to determine amplitude equations for more general patterns of the form

$$g_1(\mathbf{r}, \tau) = \sum_{j=1}^{N} A_j(\tau)\mathrm{e}^{ip_c\mathbf{R}_j\cdot\mathbf{r}}, \tag{80}$$

(and see (47) – (49)). For further discussion we refer the reader to [31, 66].

2.3 Brain wave equations

Apart from the *weakly nonlinear analysis* described above there are very few other techniques for analytically investigating neural field models (apart from maybe symmetric bifurcation theory and the use of piece-wise linear firing rate functions – of which we shall say more later). One natural step is therefore to make use of numerical simulations to explore system dynamics. For homogeneous models we may exploit the convolution structure of interactions to develop fast Fourier methods to achieve this. Indeed we may also exploit this structure further to obtain equivalent PDE models [51], and recover the Brain wave equation often used in EEG modelling [55, 45].

For example consider a one-dimensional neural field model with axonal delays:

$$Qg = \psi, \qquad \psi(x,t) = \int_{-\infty}^{\infty} \mathrm{d}y w(|x-y|) f(g(y, t-|x-y|)/v). \tag{81}$$

The function $\psi(x,t)$ may be expressed in the form

$$\psi(x,t) = \int_{-\infty}^{\infty} \mathrm{d}s \int_{-\infty}^{\infty} \mathrm{d}y G(x-y, t-s)\rho(y,s), \tag{82}$$

where

$$G(x,t) = \delta(t-|x|/v)w(x), \tag{83}$$

can be interpreted as another type of Green's function, and we use the notation

$$\rho(x,t) = f(g(x,t)). \tag{84}$$

Introducing Fourier transforms of the following form

$$\psi(x,t) = \frac{1}{(2\pi)^2}\int_{-\infty}^{\infty}\int_{-\infty}^{\infty} \mathrm{e}^{i(kx+\omega t)}\psi(k,\omega)\mathrm{d}k\mathrm{d}\omega, \tag{85}$$

allows us to write

$$\psi(k,\omega) = G(k,\omega)\rho(k,\omega), \tag{86}$$

assuming the Fourier transform of $f(u)$ exists. It is straightforward to show that the Fourier transform of (83) is

$$G(k,\omega) = \nu(\omega/v + k) + \nu(\omega/v - k), \tag{87}$$

where

$$\nu(E) = \int_0^{\infty} w(x)\mathrm{e}^{-iEx}\mathrm{d}x. \tag{88}$$

We shall focus on a common form of (normalised) exponential synaptic footprint:

$$w(x) = \frac{1}{2\sigma}\exp(-|x|/\sigma), \qquad \nu(E) = \frac{1}{2\sigma}\frac{1}{\sigma^{-1}+iE}, \qquad \sigma > 0. \tag{89}$$

We now exploit the product structure of (86) and properties of (87) to re-formulate the original integral model in terms of a partial differential equation. Using (87) and (89) we see that

$$G(k,\omega) = \frac{1}{\sigma}\frac{A(\omega)}{A(\omega)^2+k^2}, \qquad A(\omega) = \frac{1}{\sigma} + i\frac{\omega}{v}. \tag{90}$$

We may now write (86) as $(A(\omega)^2 + k^2)\psi(k,\omega) = A(\omega)\rho(k,\omega)/\sigma$, which upon inverse Fourier transforming gives the PDE:

$$\left[\mathcal{A}^2 - \partial_{xx}\right]\psi = \frac{1}{\sigma}\mathcal{A}\rho, \qquad \mathcal{A} = \left(\frac{1}{\sigma} + \frac{1}{v}\partial_t\right). \tag{91}$$

This is a type of damped wave equation with an inhomogeneity dependent on (84). This equation has previously been derived by Jirsa and Haken [45] and studied intensively in respect to the brain-behaviour experiments of Kelso *et al.* [46]. For the numerical analysis of travelling wave solutions to (91) we refer the reader to [24].

The same approach can also be used in two spatial dimensions – and here $G(k,\omega) = G(\mathbf{k},\omega)$ would be interpreted as the three dimensional integral transform:

$$G(k,\omega) = \int_{-\infty}^{\infty}\mathrm{d}s\int_{\mathbb{R}^2}\mathrm{d}\mathbf{r}G(\mathbf{r},s)\mathrm{e}^{-i(\mathbf{k}\cdot\mathbf{r}+\omega s)}. \tag{92}$$

For the choice $w(r) = \mathrm{e}^{-r/\sigma}/(2\pi)$, we find that

$$G(k,\omega) = \frac{A(\omega)}{(A^2(\omega)+k^2)^{3/2}}, \tag{93}$$

which, unlike in one spatial dimension, is not a ratio of polynomials in k and ω. The problem arises as how to interpret $[\mathcal{A}^2 - \nabla^2]^{3/2}$. In the long-wavelength approximation one merely expands $G(k,\omega)$ around $k = 0$ for small k, yielding a "nice" rational polynomial structure which is then manipulated as described above to give the PDE:

$$\left(\mathcal{A}^2 - \frac{3}{2}\nabla^2\right)\psi = \rho. \tag{94}$$

This model has been intensively studied by a number of authors in the context of EEG modelling, see for example [65, 59, 5]. For an alternative approximation to the long-wavelength one we refer the reader to [28].

Calculation of $G(\mathbf{k},\omega) = G(|\mathbf{k}|,\omega)$ for $w(r) = \exp(-r/\sigma)/(2\pi)$

$$\begin{aligned} G(k,\omega) &= (2\pi)^{-1} \int_{-\infty}^{\infty} \mathrm{d}s \int_{\mathbb{R}^2} \mathrm{d}\mathbf{r} \mathrm{e}^{-|\mathbf{r}|/\sigma} \delta(s - |\mathbf{r}|/v) \mathrm{e}^{-i(\mathbf{k}\cdot\mathbf{r}+\omega s)}, \\ &= (2\pi)^{-1} \int_0^{2\pi} \int_0^{\infty} \mathrm{e}^{-ikr\cos\theta} \mathrm{e}^{-Ar} r \mathrm{d}r \mathrm{d}\theta = -(2\pi)^{-1} \frac{\partial}{\partial A} \int_0^{2\pi} \frac{1}{A + ik\cos\theta} \mathrm{d}\theta, \qquad A(\omega) = \frac{1}{\sigma} + i\frac{\omega}{v}. \end{aligned}$$

This may be evaluated using a (circular) contour integral in the complex plane and gives

$$G(k,\omega) = \frac{A(\omega)}{(A(\omega)^2 + k^2)^{3/2}}.$$

3 Lecture 3

3.1 Travelling waves and localised states

The sorts of dynamic behaviour that are typically observed in neural field models includes, spatially and temporally periodic patterns (beyond a Turing instability) (see previous discussion), localised regions of activity (bumps and multi-bumps) [52, 48] and travelling waves (fronts, pulses, target waves and spirals) [34, 58, 44]. In the latter case corresponding phenomena may be observed experimentally using multi-electrode recordings and imaging methods. In particular it is possible to electrically stimulate slices of pharmacologically treated tissue taken from the cortex [17, 39, 70], hippocampus [54] and thalamus [47]. In brain slices these waves can take the form of spindle waves seen at the onset of sleep [64], the propagation of synchronous discharge during an epileptic seizure [20] and waves of excitation associated with sensory processing [33]. Interestingly, spatially localised bumps of activity have been linked to working memory (the temporary storage of information within the brain) in prefrontal cortex [19, 38], representations in the head-direction system [71], and feature selectivity in the visual cortex, where bump formation is related to the *tuning* of a particular neuron's response [4].

Here we shall show how to calculate the properties of waves and bumps for the special case of a Heaviside firing rate function, $f(g) = H(g-h)$, for some constant threshold h. For clarity of exposition we shall focus on a one-dimensional neural field model with axonal delays:

$$g(x,t) = \int_{-\infty}^{\infty} \mathrm{d}y w(y) \int_0^{\infty} \mathrm{d}s \eta(s) f \circ g(x-y, t-s-|y|/v). \tag{95}$$

3.2 Construction and stability (Evans functions)

Following the standard approach for constructing travelling wave solutions to PDEs, such as reviewed by Sandstede [60], we introduce the coordinate $\xi = x - ct$ and seek functions $U(\xi,t) = g(x-ct,t)$ that satisfy (95). In the (ξ,t) coordinates, the integral equation (95) reads

$$U(\xi,t) = \int_{-\infty}^{\infty} \mathrm{d}y w(y) \int_0^{\infty} \mathrm{d}s \eta(s) f \circ U(\xi - y + cs + c|y|/v, t-s-|y|/v). \tag{96}$$

The travelling wave is a stationary solution $U(\xi,t) = q(\xi)$ (independent of t), that satisfies

$$q(\xi) = \int_0^{\infty} \eta(s)\psi(\xi+cs)\mathrm{d}s, \qquad \psi(\xi) = \int_{-\infty}^{\infty} w(y) f \circ q(\xi - y + c|y|/v)\mathrm{d}y. \tag{97}$$

To determine stability we linearise (96) about the steady state $q(\xi)$ by writing $U(\xi,t) = q(\xi) + u(\xi,t)$, and Taylor expand, to give

$$u(\xi,t) = \int_{-\infty}^{\infty} \mathrm{d}y w(y) \int_0^{\infty} \mathrm{d}s \eta(s) f'(q(\xi - y + cs + c|y|/v)) u(\xi - y + cs + c|y|/v, t-s-|y|/v). \tag{98}$$

Of particular importance are bounded smooth solutions defined on $\mathbb{R}$, for each fixed t. Thus one looks for solutions of the form $u(\xi,t) = u(\xi)\mathrm{e}^{\lambda t}$. This leads to the eigenvalue equation $u = \mathcal{L}u$:

$$u(\xi) = \int_{-\infty}^{\infty} \mathrm{d}y w(y) \int_{\xi - y + c|y|/v}^{\infty} \frac{\mathrm{d}s}{c} \eta(-\xi/c + y/c - |y|/v + s/c) \mathrm{e}^{-\lambda(-\xi/c + y/c + s/c)} f'(q(s)) u(s). \tag{99}$$

Let $\sigma(\mathcal{L})$ be the spectrum of $\mathcal{L}$. We shall say that a travelling wave is linearly stable if

$$\max\{\mathrm{Re}(\lambda) : \lambda \in \sigma(\mathcal{L}),\ \lambda \neq 0\} \leq -K, \tag{100}$$

for some $K > 0$, and $\lambda = 0$ is a simple eigenvalue of $\mathcal{L}$. In general the normal spectrum of the operator obtained by linearising a system about its travelling wave solution may be associated with the zeros of a complex analytic function, the so-called Evans function. This was originally formulated by Evans [35] in the context of a stability theorem about excitable nerve axon equations of Hodgkin-Huxley type.

3.2.1 Travelling front

As an example consider travelling front solutions such that $q(\xi) > h$ for $\xi < 0$ and $q(\xi) < h$ for $\xi > 0$. It is then a simple matter to show that

$$\psi(\xi) = \begin{cases} \int_{\xi/(1-c/v)}^{\infty} w(y)\mathrm{d}y & \xi \geq 0 \\ \int_{\xi/(1+c/v)}^{\infty} w(y)\mathrm{d}y & \xi < 0 \end{cases}. \tag{101}$$

The choice of origin, $q(0) = h$, gives an implicit equation for the speed of the wave as a function of system parameters.

The construction of the Evans function begins with an evaluation of (99). Under the change of variables $z = q(s)$ this equation may be written

$$u(\xi) = \int_{-\infty}^{\infty} \mathrm{d}y w(y) \int_{q(\xi - y + c|y|/v)}^{q(\infty)} \frac{\mathrm{d}z}{c} \eta(q^{-1}(z)/c - \xi/c + y/c - |y|/v) \\ \mathrm{e}^{-\lambda(q^{-1}(z)/c - \xi/c + y/c)} \times \frac{\delta(z-h)}{|q'(q^{-1}(z))|} u(q^{-1}(z)). \tag{102}$$

For the travelling front of choice we note that when $z = h$, $q^{-1}(h) = 0$ and (102) reduces to

$$u(\xi) = \frac{u(0)}{c|q'(0)|} \int_{-\infty}^{\infty} \mathrm{d}y w(y) \eta(-\xi/c + y/c - |y|/v) \mathrm{e}^{-\lambda(y-\xi)/c}. \tag{103}$$

From this equation we may generate a self-consistent equation for the value of the perturbation at $\xi = 0$, simply by setting $\xi = 0$ on the left hand side of (103). This self-consistent condition reads

$$u(0) = \frac{u(0)}{c|q'(0)|} \int_{-\infty}^{\infty} \mathrm{d}y w(y) \eta(y/c - |y|/v) \mathrm{e}^{-\lambda y/c}. \tag{104}$$

Importantly there are only nontrivial solutions if $\mathcal{E}(\lambda) = 0$, where

$$\mathcal{E}(\lambda) = 1 - \frac{1}{c|q'(0)|} \int_{-\infty}^{\infty} \mathrm{d}y w(y) \eta(y/c - |y|/v) \mathrm{e}^{-\lambda y/c}. \tag{105}$$

From causality $\eta(t) = 0$ for $t \leq 0$ and physically $c < v$ so

$$\mathcal{E}(\lambda) = 1 - \frac{1}{c|q'(0)|} \int_{0}^{\infty} \mathrm{d}y w(y) \eta(y/c - y/v) \mathrm{e}^{-\lambda y/c}. \tag{106}$$

We identify (106) with the Evans function for the travelling front solution of (95). The Evans function is real-valued if λ is real. Furthermore, (i) the complex number λ is an eigenvalue of the operator $\mathcal{L}$ if and only if $\mathcal{E}(\lambda) = 0$, and (ii) the algebraic multiplicity of an eigenvalue is equal to the order of the zero of the Evans function.

Here we consider the choice $\eta(t) = \alpha \mathrm{e}^{-\alpha t}$ and $w(x) = \mathrm{e}^{-|x|}/2$. Assuming $c > 0$ the travelling front (97) is given in terms of (101) which takes the explicit form

$$\psi(\xi) = \begin{cases} \frac{1}{2}\mathrm{e}^{m_- \xi} & \xi \geq 0 \\ 1 - \frac{1}{2}\mathrm{e}^{m_+ \xi} & \xi < 0 \end{cases}, \qquad m_\pm = \frac{v}{c \pm v}. \tag{107}$$

The speed of the front is determined from the condition $q(0) = h$ as

$$c = \frac{v(2h-1)}{2h-1-2hv/\alpha}. \tag{108}$$

The Evans function is easily calculated as

$$\mathcal{E}(\lambda) = \frac{\lambda}{c + \alpha\,(1 - c/v) + \lambda}, \tag{109}$$

where we use the result from (97) and (101) that $cq'(0) = \int_0^\infty \eta(y/c - y/v)w(y)\mathrm{d}y$. The equation $\mathcal{E}(\lambda) = 0$ only has the solution $\lambda = 0$. We also have that $\mathcal{E}'(0) > 0$ showing that $\lambda = 0$ is a simple eigenvalue. Hence, the travelling wave front for this example is linearly stable.

We refer the reader to [25] for further examples of wave calculations in other neural field models.

3.2.2 Stationary bump

Here we construct static (time-independent) patterns of the form $g(x,t) = q(x)$ for all t. Using (95) gives

$$q(x) = \int_{-\infty}^{\infty} w(x-y)H(q(y) - h)\mathrm{d}y. \tag{110}$$

We shall assume the synaptic kernel has a Mexican hat shape given by

$$w(x) = (1 - |x|)\mathrm{e}^{-|x|}, \tag{111}$$

and look for solutions of the form $\lim_{x\to\pm\infty} q(x) = 0$, with $q(x) \geq h$ for $x_1 < x < x_2$ (see inset of Fig. 2). In this case the exact solution is given simply by

$$q(x) = \int_{x_1}^{x_2} w(x-y)\mathrm{d}y. \tag{112}$$

For the Mexican hat function (111), a simple calculation gives

$$q(x) = \begin{cases} g(x-x_1) - g(x-x_2) & x > x_2 \\ g(x_2-x) + g(x-x_1) & x_1 \leq x \leq x_2 \\ g(x_2-x) - g(x_1-x) & x < x_1 \end{cases}, \tag{113}$$

where $g(x) = x\mathrm{e}^{-x}$. The conditions $q(x_1) = h$ and $q(x_2) = h$ both lead to the equation

$$\Delta\mathrm{e}^{-\Delta} = h, \tag{114}$$

describing a family of solutions with $\Delta = (x_2 - x_1)$. Hence, homoclinic bumps are only possible if $h < 1/\mathrm{e}$. The full branch of solutions for $\Delta = \Delta(h)$ is shown in Fig. 2. Here we see a branch of wide solutions ($\Delta > 1$) and a branch of thinner solutions ($\Delta < 1$) that connect in a saddle-node bifurcation at $\Delta = 1$. One of the translationally invariant solutions may be picked by imposing a *phase* condition $q(0) = q_0$, where $q_0 \leq \max q(x) = \Delta\mathrm{e}^{-\Delta/2}$ (which occurs at $(x_1 + x_2)/2$ using (113)).

To determine stability we use the result that $q'(x) = w(x-x_1) - w(x-x_2)$ so that the eigenvalue equation (99), with $c = 0$, reduces to

$$u(x) = \frac{\widetilde{\eta}(\lambda)}{|w(0) - w(\Delta)|}[w(x-x_1)u(x_1)\mathrm{e}^{-\lambda|x-x_1|/v} + w(x-x_2)u(x_2)\mathrm{e}^{-\lambda|x-x_2|/v}], \tag{115}$$

s

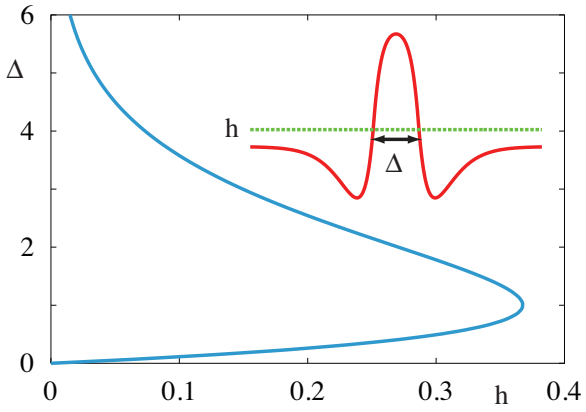

Figure 2: Bump width as a function of h, as determined by equation (114) for a step function firing rate function and Mexican hat kernel (111). The inset shows the shape of a bump.

where $\widetilde{\eta}(\lambda) = \int_0^\infty \eta(s)\mathrm{e}^{-\lambda s}\mathrm{d}s$. The equality in (115) implies that if $u(x_{1,2}) = 0$ then $u(x) = 0$ for all x. We now examine the matrix equation obtained from (115) at the points $x = x_{1,2}$,

$$\begin{bmatrix} u(x_1) \\ u(x_2) \end{bmatrix} = \frac{\widetilde{\eta}(\lambda)}{|w(0) - w(\Delta)|} \begin{bmatrix} w(0) & w(\Delta)\mathrm{e}^{-\lambda|\Delta|/v} \\ w(\Delta)\mathrm{e}^{-\lambda|\Delta|/v} & w(0) \end{bmatrix} \begin{bmatrix} u(x_1) \\ u(x_2) \end{bmatrix}. \tag{116}$$

Non-trivial solutions are only possible if

$$\frac{1}{\widetilde{\eta}(\lambda)} = \frac{w(0) \pm w(\Delta)\mathrm{e}^{-\lambda|\Delta|/v}}{|w(0) - w(\Delta)|}. \tag{117}$$

Solutions will be stable if $\mathrm{Re}(\lambda) < 0$. It is a simple matter to check that there is always one solution with $\lambda = 0$. For an exponential synapse $\widetilde{\eta}(\lambda) = (1 + \lambda/\alpha)^{-1}$ and we see that as $v \to \infty$ solutions are only stable if $(w(0) + w(\Delta))/|w(0) - w(\Delta)| < 1$. This is true if $w(\Delta) = \exp(-\Delta)(1 - \Delta) < 0$. Hence, of the two possible branches of $\Delta = \Delta(h)$, it is the one with largest Δ that is stable. In the other extreme where $v \to 0$ it is simple to show that real and positive values for λ can only occur when $w(\Delta) > 0$. Hence, as v is varied there are no new instabilities due to real eigenvalues passing through zero. However, for finite conduction velocities it is possible that solutions may destabilise via a Hopf bifurcation. By writing $\lambda = i\omega$ the conditions for a Hopf bifurcation, where $\mathrm{Re}(\lambda) = 0$ and $\mathrm{Im}(\lambda) \neq 0$, are obtained from the simultaneous solution of

$$1 = \frac{w(0) + w(\Delta)\cos(\omega|\Delta|/v)}{|w(0) - w(\Delta)|}, \qquad \frac{\omega}{\alpha} = -\frac{w(\Delta)\sin(\omega|\Delta|/v)}{|w(0) - w(\Delta)|}. \tag{118}$$

Eliminating $\sin(\omega|\Delta|/v)$ between these two equations gives

$$\omega^2 = \frac{\alpha^2}{|w(0) - w(\Delta)|^2}\left[w^2(\Delta) - \{|w(0) - w(\Delta)| - w(0)\}^2\right]. \tag{119}$$

The condition that $\omega \neq 0$ requires the choice $w(\Delta) > w(0)$, which does not hold for (111). Hence, the presence of axonal delays neither affects the existence or stability of bump solutions.

3.3 Interface dynamics

For zero axonal delays ($v \to \infty$) and $\eta(t) = \alpha\mathrm{e}^{-\alpha t}H(t)$ the existence and stability of bumps may be investigated using the alternative techniques of Amari [2]. We use the threshold condition $g(x_i, t) = h$ to define the locations

$x_{1,2}$ from which we obtain the equations of motion of the boundary as

$$\frac{\mathrm{d}x_i}{\mathrm{d}t} = -\left.\frac{g_t}{g_x}\right|_{x=x_i(t)}. \tag{120}$$

It is then possible to calculate the rate of change of the interval $\Delta(t) = x_2(t) - x_1(t)$ using

$$\frac{1}{\alpha} g_t(x,t) = -g(x,t) + \int_{x_1(t)}^{x_2(t)} w(x-y)\mathrm{d}y. \tag{121}$$

Then (for a single bump)

$$\frac{\mathrm{d}\Delta}{\mathrm{d}t} = \alpha\left(\frac{1}{c_1} + \frac{1}{c_2}\right)\left[\int_0^{\Delta} w(|y|)\mathrm{d}y - h\right], \tag{122}$$

where

$$c_1 = \frac{\partial g(x_1,t)}{\partial x}, \qquad -c_2 = \frac{\partial g(x_2,t)}{\partial x}. \tag{123}$$

Hence, making the convenient assumption that $\partial g(x_i,t)/\partial x$ is roughly constant, the equilibrium solution defined by $\int_0^{\Delta} w(|y|)\mathrm{d}y = h$ is stable if

$$\frac{\mathrm{d}}{\mathrm{d}\Delta}\int_0^{\Delta} w(|y|)\mathrm{d}y = w(\Delta) < 0. \tag{124}$$

We thus recover the result obtained with the Evans function method (widest bump is stable).

It is also possible to recover results about travelling fronts in the interface framework (at least for $v \to \infty$). In this case it is natural to define a pattern boundary as the interface between a high and low activity state. Let us assume that the front is such that $g(x,t) > h$ for $x < x_0(t)$ and $g(x,t) \leq h$ for $x \geq x_0(t)$ then (95), for the choice $\eta(t) = \mathrm{e}^{-t}H(t)$, reduces to

$$g_t(x,t) = -g(x,t) + \int_{x-x_0(t)}^{\infty} w(y)\mathrm{d}y. \tag{125}$$

Introducing $z = u_x$ and differentiating (125) with respect to x gives

$$z_t(x,t) = -z(x,t) - w(x - x_0(t)). \tag{126}$$

Integrating (126) from $-\infty$ to t (and dropping transients) gives

$$z(x,t) = -\mathrm{e}^{-t}\int_{-\infty}^{t} \mathrm{e}^{s} w(x - x_0(s))\mathrm{d}s. \tag{127}$$

We may now use the interface dynamics, $g(x_0(t),t)$, defined by:

$$\dot{x}_0 = -\left.\frac{g_t}{g_x}\right|_{x=x_0(t)}, \tag{128}$$

to study the speed $c > 0$ of a front, defined by $\dot{x}_0 = c$. In this case $x_0(t) = ct$ (where without loss of generality we set $x_0(0) = 0$) and from (125) and (126) we have that

$$g_t|_{x=x_0(t)} = -h + \widetilde{w}(0), \qquad g_x|_{x=x_0(t)} = -\widetilde{w}(1/c)/c, \tag{129}$$

where $\widetilde{w}(\lambda) = \int_0^{\infty} \mathrm{e}^{-\lambda s} w(s)\mathrm{d}s$. Hence from (128) the speed of the front is given implicitly by the equation

$$h = \widetilde{w}(0) - \widetilde{w}(1/c). \tag{130}$$

To determine stability of the travelling wave we consider a perturbation of the interface and an associated perturbation of g. Introducing the notation $\widehat{\cdot}$ to denote perturbed quantities to a first approximation we will

set $\widehat{g}_x|_{x=\widehat{x}_0(t)} = g_x|_{x=ct}$, and write $\widehat{x}_0(t) = ct + \delta x_0(t)$. The perturbation in g can be related to the perturbation in the interface by noting that the perturbed and unperturbed boundaries are defined by a level set condition so that $g(x_0, t) = h = \widehat{g}(\widehat{x}_0, t)$. Introducing $\delta g(t) = g|_{x=ct} - \widehat{g}|_{x=\widehat{x}_0(t)}$ we thus have the condition that $\delta g(t) = 0$ for all t. Integrating (125) (and dropping transients) gives

$$g(x,t) = \mathrm{e}^{-t} \int_{-\infty}^{t} \mathrm{d}s \mathrm{e}^{s} \int_{x-x_0(s)}^{\infty} \mathrm{d}y w(y), \tag{131}$$

and $\widehat{g}$ is obtained from (131) by simply replacing x_0 by $\widehat{x}_0$. Using the above we find that δu is given (to first order in δx_0) by

$$\delta g(t) = \frac{1}{c} \int_0^{\infty} \mathrm{d}s \mathrm{e}^{-s/c} w(s)[\delta x_0(t) - \delta x_0(t - s/c)] = 0. \tag{132}$$

This has solutions of the form $\delta x_0(t) = \mathrm{e}^{\lambda t}$, where λ is defined by $\mathcal{E}(\lambda) = 0$, with

$$\mathcal{E}(\lambda) = 1 - \frac{\widetilde{w}((1+\lambda)/c)}{\widetilde{w}(1/c)}. \tag{133}$$

A front is stable if Re$\lambda < 0$.

As an example consider the choice $w(x) = \exp(-|x|/\sigma)/2$, for which $\widetilde{w}(\lambda) = (\lambda + 1/\sigma)^{-1}/(2\sigma)$. In this case the speed of the wave is given from (130) as

$$c = \frac{1-2h}{2h}, \tag{134}$$

and

$$\mathcal{E}(\lambda) = \frac{\lambda}{1+c+\lambda}. \tag{135}$$

The equation $\mathcal{E}(\lambda) = 0$ only has the solution $\lambda = 0$. We also have that $\mathcal{E}'(\lambda) > 0$, showing that $\lambda = 0$ is a simple eigenvalue. Hence, the travelling wave front for this example is neutrally stable.

For a recent extension of the Amari interface dynamics to planar neural field models we refer the reader to [26].

4 Lecture 4

4.1 Waves in random neural media

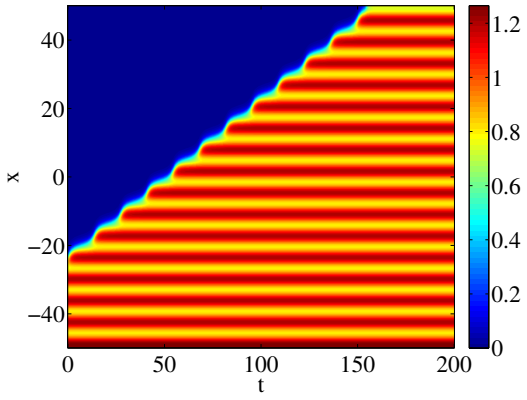

Many neural field models make the assumption that the synaptic weight distribution only depends upon the distance between interacting populations. For example, in (15) we would take $w(x,y) = w(|x-y|)$. This implies translation symmetry of the underlying tissue. From a mathematical perspective this is particularly useful for analysing travelling waves, which can be constructed as stationary profiles in a co-moving frame. In the special case that f is a Heaviside function then the dependence of wave speed and stability on the shape of the homogeneous connectivity can be analysed exactly (see above). However, analogous results for heterogeneous systems are much harder to come by and even the existence and uniqueness of solutions to (15) has only been treated recently [36]. For the particular case that the connectivity has the form $w(x,y) = w(|x-y|)[1+\sigma K(y/\sigma)]$ with K some periodic function, which models the *patchiness* of connections seen in cortex, Bressloff [9] has shown how averaging methods (homogenisation) can be tailored to treat non-local neural models like (15) and allow for the analysis of waves in the limit $\sigma \to 0$. Moreover, he was able to obtain explicit results for wave speeds and the conditions for propagation failure in the case of a Heaviside firing rate. For this special case Schmidt *et al*. [61] and later Coombes and Laing [26] were able to obtain improved results valid away from the limit $\sigma = 0$. The analysis of waves in truly inhomogeneous (as opposed to periodically modulated) neural media is a much harder problem, though one that will have a huge bearing on our understanding of how waves propagate throughout the brain. For a recent discussion we refer the reader to [23].

4.1.1 Pulsating fronts in a periodically modulated neural field – an interface approach

Let us first consider a simple neural field of the form

$$g_t = -g + \psi, \quad \psi(x,t) = \int_{-\infty}^{\infty} \mathrm{d}y w(x,y) H(g(y,t)-h), \tag{136}$$

with a very specific form of heterogeneity, namely one where the connectivity has the following product structure:

$$w(x,y) = w(|x-y|)[1+\epsilon K(y)], \qquad K(y) = K(y+\sigma), \tag{137}$$

and K is some σ-periodic function. The use of periodically modulated translationally-invariant kernels of this form is particularly relevant to modelling primary visual cortex, which is known to have a periodic microstructure on the millimeter scale, reviewed in some detail in the paper by Bressloff [9]. To provide a sense of the type of solutions that the model can support we first present a direct numerical simulation for the choice

$$w(x) = \frac{1}{2}\mathrm{e}^{-|x|}, \qquad K(x) = \sin(2\pi x/\sigma). \tag{138}$$

The figure above shows a space-time plot of $g(x,t)$ and a wave that connects a low activity state to a high activity state (for $\epsilon = 0.4$, $h = 0.3$ and $\sigma = 2\pi$). Although there is an easily identified front that separates these

two states it does not travel with constant speed and in fact oscillates periodically in a co-moving frame. In the wake of the front one also sees a periodic spatial pattern. We call such a wave a pulsating front. Numerical simulations show that with increasing ϵ such fronts can fail to propagate, instead becoming pinned. Motivated by the form of the pulsating front we seek to describe the properties of this solution solely in terms of the behaviour at the front edge which separates high activity from low. If the front is not pulsating (which is the case in the absence of period modulation of the connectivity) then in a travelling wave frame (of the same speed as the wave) the rising edge of the front may be identified with a single (travelling wave) co-ordinate. For a pulsating front this point is no longer stationary in time and instead oscillates. We now show how to derive the dynamics for this *interface* between high and low activity states.

In a co-moving frame the model (136) takes the form $g = g(\xi, t)$ where $\xi = x - c_0 t$ for some fixed c_0 and

$$-c_0 g_\xi + g_t = -g + \psi, \tag{139}$$

where

$$\psi(\xi, t) = \int_{-\infty}^{\infty} \mathrm{d}y w(\xi + c_0 t, y) H(g(y - c_0 t, t) - h). \tag{140}$$

We define a moving interface (level set) according to

$$u(\xi_0(t), t) = h. \tag{141}$$

Here we are assuming that there is only one point on the interface (though in principle we could consider a set of points). Differentiation of (141) gives an exact expression for the velocity of the interface in the form

$$\dot{\xi}_0 = -\left.\frac{g_t}{g_\xi}\right|_{\xi=\xi_0(t)}. \tag{142}$$

Focusing now on a solution with $g > h$ for $\xi < \xi_0$ (140) takes the simple form

$$\psi(\xi, t) = \int_{-\infty}^{\xi_0 + c_0 t} \mathrm{d}y w(\xi + c_0 t, y). \tag{143}$$

For $\epsilon = 0$ there is a travelling front $q(\xi)$ given by the solution of

$$-c_0 \frac{\mathrm{d}q}{\mathrm{d}\xi} = -q + \psi, \qquad \psi(\xi) = \int_{\xi}^{\infty} \mathrm{d}y w(|y|), \tag{144}$$

where the speed c_0 is determined by $q(0) = h$ (and see also section 3.3). For small ϵ we assume that the slope of the travelling front varies sufficiently slowly so that we may make the convenient approximation $u_\xi|_{\xi=\xi_0(t)} = q_\xi|_{\xi=0}$. In this case we have, using equations (139) and (144), that

$$g_t|_{\xi=\xi_0(t)} = \int_{-\infty}^{\xi_0 + c_0 t} \mathrm{d}y w(\xi_0 + c_0 t, y) - \int_0^{\infty} \mathrm{d}y w(|y|), \tag{145}$$

$$g_\xi|_{\xi=\xi_0(t)} = \frac{1}{c_0}\left(h - \int_0^{\infty} \mathrm{d}y w(|y|)\right). \tag{146}$$

Substitution of equations (145) and (146) into equation (142) gives

$$\dot{\xi}_0 = \epsilon c_0 \frac{\int_0^{\infty} \mathrm{d}y w(|y|) K(\xi_0 + c_0 t - y)}{h - \int_0^{\infty} \mathrm{d}y w(|y|)}. \tag{147}$$

For the choice (138) the time-dependent speed of the front is then given by $c_0(1 + \epsilon a(\xi_0, t))$ where $c_0 = (1 - 2h)/(2h)$ and

$$a(\xi_0, t) = A \sin\left[\frac{2\pi}{\sigma}(\xi_0 + c_0 t) - \phi\right], \tag{148}$$

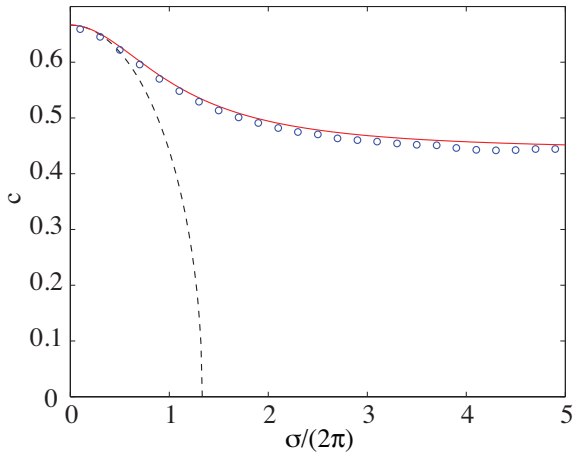

Figure 3: Red solid line: the result from an interface dynamics analysis given by equation (152). Circles show results measured from simulations. Black dashed line: the result from homogenisation theory given by equation (153). Parameters are $\epsilon = 0.3$ and $h = 0.3$.

with

$$A = \frac{1}{2h-1}\frac{1}{\sqrt{1+(2\pi/\sigma)^2}}, \quad \tan\phi = \frac{2\pi}{\sigma}. \tag{149}$$

Pulsating fronts are T-periodic solutions of the non-autonomous ordinary differential equation (147) with $\xi_0(t) = \xi_0(t+T)$. Introducing $x_0 = \xi_0 + c_0 t$ with $x_0 \in [0, \sigma]$ we may solve for the trajectory using:

$$\int_0^{x_0} \frac{\mathrm{d}x}{1+\epsilon A \sin(2\pi x/\sigma - \phi)} = c_0 t. \tag{150}$$

Using a half angle substitution we may evaluate this to give

$$c_0 t = \frac{\sigma}{\pi}\frac{1}{\alpha}\tan^{-1}\frac{z}{\alpha}\Big|_{z_0(0)+\epsilon A}^{z_0(t)+\epsilon A}, \qquad \alpha^2 = 1-\epsilon^2 A^2, \tag{151}$$

where $z_0(t) = \tan[(2\pi x_0(t)/\sigma - \phi)/2]$ and $x_0(0) = 0$. A periodic pulsating front with speed $c = \sigma/T$ can be found by demanding that $\sigma = x_0(T)$. Substitution of this condition into (151) shows that the speed of the pulsating front is given by

$$c = c_0\sqrt{1-\epsilon^2 A^2}. \tag{152}$$

Hence, a propagating wave is only supported if $|\epsilon| < 1/|A|$.

A plot of the wave speed as a function of the spatial scale σ is shown in Fig. 3. We see excellent agreement between the theoretical prediction from the interface dynamics approach and direct numerical simulations. Although our analysis in this case is restricted to small ϵ we have not had to make any assumptions about the scale of periodic modulation as determined by the parameter σ. In contrast a homogenisation analysis would require both small ϵ *and* a periodic modulation that occurs on a smaller length-scale than the correlation length of $w(x)$ (which is set to unity here). Following the calculation by Bressloff in [9] an application of homogenisation theory gives

$$c = c_0\sqrt{1-\epsilon^2 B^2}, \qquad B = \frac{1}{2h-1}\frac{\sigma}{2\pi}. \tag{153}$$

As expected the result from the interface approach equation (152) recovers that from homogenisation theory, given by (153), in the limit $\sigma \to 0$. However, as illustrated in Fig. 3 the homogenisation result gives poor results for σ away from zero.

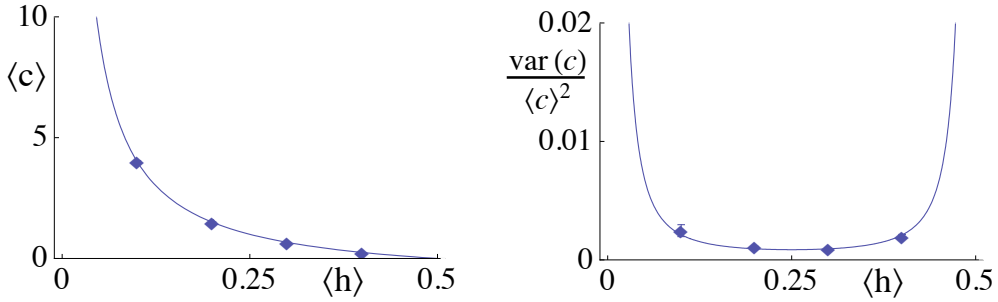

Figure 4: Mean (left) and scaled variance (right) of the wave front speed as a function of the threshold. $\langle \delta h(x)^2 \rangle_x = 1.35 \times 10^{-5}$.

4.1.2 Threshold fluctuation

For a Heaviside firing rate function Brackley and Turner [7] have considered temporal correlations in a fluctuating threshold (taken to be a Gaussian random variable). Using a mixture of numerics and analysis they investigated how temporal correlations in the threshold affected the shape and speed of wave fronts. Here we pursue a similar analysis, focusing on a homogenous kernel with $w(x, y) = \exp(-|x - y|)/2$, and analyse the effects of spatial correlations in the threshold. The firing threshold $h(x)$ is chosen to fluctuate around a mean value $\overline{h}$, such that $h(x) = \overline{h} + \delta h(x)$ where

$$\langle \delta h(x) \rangle_x = 0, \qquad \langle \delta h(x), \delta h(x+y) \rangle_x = a \mathrm{e}^{-|y|/\nu}/(2\nu). \tag{154}$$

Choosing large ν and small a gives a small slowly varying fluctuation in the firing threshold about a mean value $\overline{h}$. In the absence of any fluctuations ($a = 0$) the speed of the front is given by $(1 - 2h)/(2h)$. Now, considering $\delta h \ll 1$, we expand (134) as

$$c = \frac{1 - 2\overline{h}}{2\overline{h}} + \frac{1}{2\overline{h}} \sum_{n=1}^{\infty} \left(-\frac{\delta h}{\overline{h}} \right)^n. \tag{155}$$

From this we may calculate the average speed as

$$\langle c \rangle = \frac{1 - 2\overline{h}}{2\overline{h}} + \frac{1}{2\overline{h}} \sum_{n=1}^{\infty} (2n-1)!! \frac{\langle \delta h^2 \rangle^n}{\overline{h}^{2n}}, \tag{156}$$

where !! denotes double factorial. The centered variance can also be found as

$$\langle (c - \langle c \rangle)^2 \rangle = \frac{1}{4\overline{h}^2} \left(\frac{\langle \delta h^2 \rangle}{\overline{h}^2} + 8 \frac{\langle \delta h^2 \rangle^2}{\overline{h}^4} + 69 \frac{\langle \delta h^2 \rangle^3}{\overline{h}^6} + \dots \right). \tag{157}$$

Plots of $\langle c \rangle$ and $\langle (c - \langle c \rangle)^2 \rangle / \langle c \rangle^2$ are shown in Fig. 4 using the formulas above as well as data from direct numerical simulations. We see that there is very good agreement between the small perturbation analysis and direct simulations of the model. This suggests that to a first approximation we may (for a given realisation of the threshold function) write

$$c(x) = \frac{1 - 2h(x)}{2h(x)}. \tag{158}$$

A plot of a realisation of $h(x)$ as well as the corresponding prediction from (158) and results from simulations are shown in Fig. 5, highlighting the usefulness of this simple ansatz for wave speed.

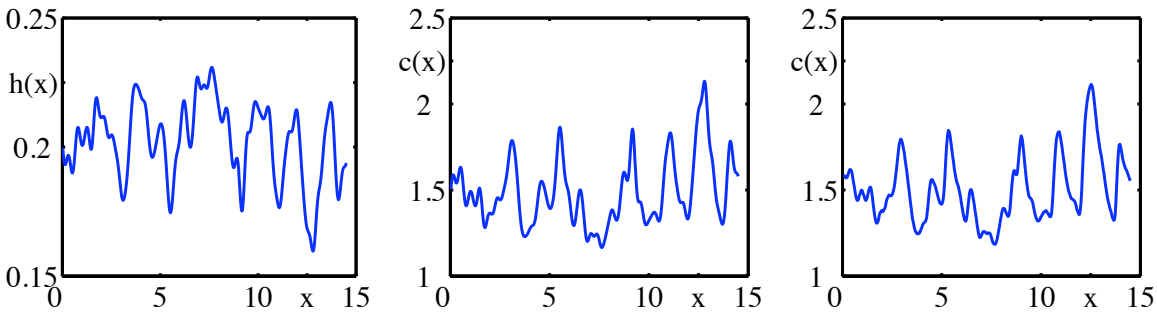

Figure 5: Left: Fluctuating firing threshold $h(x)$ for $\overline{h} = 0.2$, $a = 1$ and $\nu = 0.2$. Middle: $c(x) = (1 - 2h(x))/(2h(x))$. Right: Corresponding simulation results. (These were generated using a 4th order Runge-Kutta scheme with spatial-temporal discretisation $\Delta x = \Delta t = 0.025$ with a domain sise $N \times \Delta x = 50$ and $N = 2000$. Fast Fourier transforms were used to calculate convolution terms).

5 Lecture 5

5.1 Tissue level spiking models: the dynamics of the continuum Lighthouse model

Neural field models can go a remarkably long way to providing a framework for interpreting neuro-imaging data whilst maintaining contact with known brain structure, dynamics and function [22]. However, a well known limitation is that they only try to track mean activity levels and cannot, by definition, track the higher order correlations of any underlying spiking model. Unfortunately only in some rare instances has it been possible to analyse spiking networks directly (usually under the assumption of global coupling and fast synaptic interactions) as in the *spike-density* approach [56, 16, 3], which makes heavy use of the numerical solution of coupled partial differential-integral equations. In other situations equations going beyond the mean-field approach have been proposed that govern second-order correlations [37, 63, 6, 49]. Indeed there has been a recent upsurge of interest in this area adapting methods from non-equilibrium statistical physics to determine corrections to mean-field theory involving equations for two-point and higher-order cumulants [15, 10]. Interestingly, the Lighthouse model of Hermann Haken [40, 41] is a candidate single neuron model that may allow a bridge to be built between spiking neuron models and firing rate descriptions. Indeed in the limit of slow synaptic interactions it may be shown to reduce to the standard Amari model. Importantly the Lighthouse model is sufficiently simple that it may also be analysed at the network level, even for fast synaptic responses. Hence, a comprehensive study of a network of synaptically coupled Lighthouse neurons may pave the way for the development of a specific exactly soluble neurodynamics. This may also shed light on how best to develop a more general approach valid for more detailed models of coupled spiking neurons. Here we shall review a recent study that shows how to analyse *bump* solutions [18].

The Lighthouse model was introduced by Haken as a pulse coupled model of a spiking neural network whose behaviour could be explicitly analysed at the network level. Much is now known about phase-locked solutions and the effect of noise and delays on stability and is summarised in the book by Haken [42]. It is a hybrid between a phase-oscillator and a firing rate model. Indexing a Lighthouse neuron with $i \in \mathbb{Z}$, the dynamical description of a discrete network is cast as a system of ordinary differential equations for the phase variable $\theta_i = \theta_i(t) \in [0, 1)$, $t \in \mathbb{R}^+$, in the form

$$\frac{\mathrm{d}\theta_i}{\mathrm{d}t} = H(g_i - h), \tag{159}$$

with

$$g_i(t) = \sum_{j=1}^{N} w_{ij} E_j(t), \qquad E_i(t) = \sum_m \eta(t - T_i^m), \tag{160}$$

and H is interpreted as a firing rate function. Haken uses the Naka-Rushton sigmoidal function (though many of the analytical results for the Lighthouse model are obtained for a linear firing rate function). Here we work with the Heaviside choice. The quantity g_i is recognised as the input to neuron i, mediated by the synaptic processing of a set of incoming spikes. The spike time T_j^m marks the mth firing of neuron j, given by the times for which $\theta_j(t) = 1$. Each time neuron i fires, a synaptic pulse $\eta(t)$ (with $\eta(t) = 0$ for $t < 0$) is transmitted to other neurons $j = 1, \ldots, N$ with coupling weight w_{ij}. We shall take the synaptic response to be normalised, such that $\int_0^\infty \eta(t)\mathrm{d}t = 1$. When the input to a neuron exceeds the threshold, h, the phase will advance towards threshold at a constant rate which we have arbitrarily set to one. We note that the activity of a given neuron need not be periodic. Depending on the nature of the inputs it could also be quiescent or fire irregularly.

We consider two versions of the Lighthouse model. In the first version, which is the model originally proposed by Haken, whenever the input is below threshold or drops below threshold the phase immediately resets to zero. In this case the neuron can only fire if it receives input that remains above threshold for an entire period. In the second version the phase is not reset, except when the neuron fires. We will see that the two versions have different possible bump solutions and dynamics. In particular the instant reset version does not support *wandering* bumps.

We consider lateral inhibition-type synaptic coupling on a one dimensional lattice. The system has two length scales – the lattice spacing and the coupling footprint. We take the array length to be much longer than either of these two length scales. We can index the N neurons in the array by a distance via $x = i\delta x$, where δx is the lattice spacing. The continuum limit is given by $N \to \infty$, $\delta x \to 0$ with $\delta x N$ a constant. To make the connection to the continuum limit transparent we rewrite the coupling function as $w_{ij} = w([i-j]\delta x)\delta x$. A continuum version of the Lighthouse model (along the whole real line) is obtained under the replacement $(\theta_i, g_i, T_i^m, w((i-j)\delta x)) \to (\theta(x,t), g(x,t), T^m(x), w(x-y))$ $x \in \mathbb{R}$, and is governed by the dynamics

$$\frac{\partial \theta(x,t)}{\partial t} = H(g(x,t) - h), \tag{161}$$

with

$$g(x,t) = \sum_m \int_0^\infty \mathrm{d}s \eta(s) \int_{-\infty}^\infty \mathrm{d}y w(x-y)\delta(s - t + T^m(y)). \tag{162}$$

5.1.1 Connection to the Amari model

We first consider the continuum limit for slow synapses and show it is identical to the classical Amari model. Taking the time average of (162) gives

$$\begin{aligned}\langle g(x,t)\rangle &= \frac{1}{T}\int_t^{t+T} \mathrm{d}s \int_{-\infty}^\infty \mathrm{d}y w(x-y) \int_0^\infty \mathrm{d}s' \eta(s') \sum_m \delta(s' - s + T^m(y)) \\ &= \int_{-\infty}^\infty \mathrm{d}y w(x-y) \int_0^\infty \mathrm{d}s \eta(s) \Omega(y, t-s).\end{aligned} \tag{163}$$

where $\Omega(x,t) = M(x,t)/T$ is the firing rate and $M(x,t) = \int_t^{T+t} \sum_m \delta(s + T^m(x))\mathrm{d}s$ is the number of firing events at position x within a window T. We next recognise that the firing rate is given by

$$\Omega(x,t) = \frac{\partial \theta(x,t)}{\partial t} = H(g(x,t) - h). \tag{164}$$

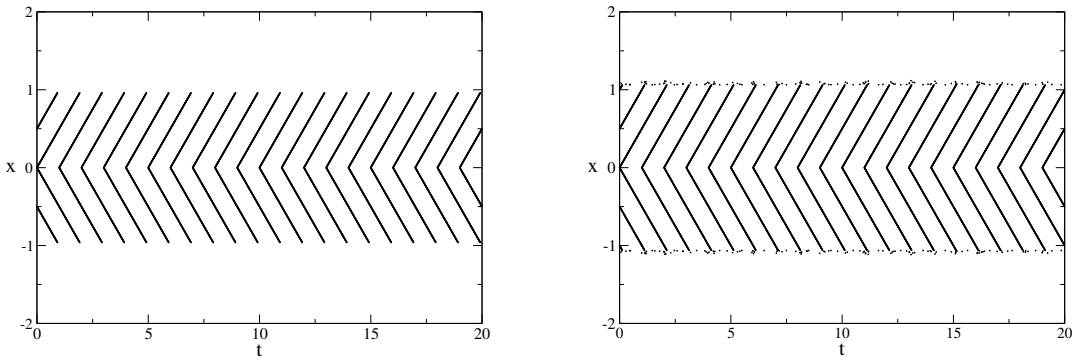

Figure 6: A direct numerical simulation of the continuum model approximated by a finite system with lattice spacing $\delta x = 0.004$ on $N = 1000$ grid points. The dots in the raster plot indicate the times of firing events. Data is shown for the parameters of Fig. 8 with $\beta = 2$. The left and right panels show results with and without phase reset respectively.

Substituting (164) into (163) gives

$$\langle g(x,t)\rangle = \int_{-\infty}^{t} \mathrm{d}s\eta(t-s) \int_{-\infty}^{\infty} \mathrm{d}y w(x-y) H(g(y,s)-h). \tag{165}$$

For slow synaptic interactions (such that $\eta(t)$ is approximately constant over the timescale T), then we have the condition $g(x,t) = \langle g(x,t)\rangle$. For the specific choice $\eta(t) = \alpha \mathrm{e}^{-\alpha t} H(t)$, (165) may be written in the form

$$\frac{1}{\alpha}\frac{\partial g(x,t)}{\partial t} = -g(x,t) + \int_{-\infty}^{\infty} \mathrm{d}y w(x-y) H(g(y,t)-h), \tag{166}$$

which is recognised as the Amari model [2]. The equivalence between the Lighthouse and Amari model is only strictly true in the limit of $\alpha \to 0$ where g is constant in time. For non-zero α we will see that the dynamics between the two models deviate substantially. Indeed if the Amari model supports bumps, then it is known that their stability is insensitive to variation in the synaptic rate parameter α (see section 3.2.2). However, in the analogous Lighthouse model although bumps exist they are not stable to variations in α.

5.1.2 Bump solutions

The Lighthouse model can support localised bump solutions that may undergo a transition to wandering. An example of a spiking bump state is shown in Fig. 6 with the left and right panels showing simulation results with and without phase reset. Similar behaviour is seen in networks of integrate-and-fire (IF) neurons [50]. Despite its seeming simplicity it is not straight-forward to analyse bumps in IF networks, though the analysis of phase-locked states has been done in [12]. In contrast the Lighthouse is much more amenable to mathematical analysis. We are interested in analysing the existence and dynamics of localised pulses of activity or bumps. A bump is defined as a group of contiguous neurons that fire together. However, given the discontinuous nature of spiking events and that the bump location may change in time it is necessary to make this idea more precise with the following definitions.

Definition 1 *A* **bump** *at time t is the set of all contiguous neurons that fired in the time interval $[t-1, t]$.*

Definition 2 *A* **stationary bump** *is a bump which persists in a single location for all time i.e. the same set of neurons continue to fire indefinitely.*

Definition 3 *An* **equiperiod bump** *is a stationary bump for which the neurons in the bump all fire with the same rate.*

We shall assume that the connectivity kernel is homogeneous ($w(x) = w(|x|)$), and work with the explicit functions $\eta(t) = \alpha \exp(-\alpha t)H(t)$ and the "wizard hat" $w(x) = A\exp(-a|x|) - \exp(-|x|)$. We first consider conditions for the existence of a continuum equiperiod bump in the limit of infinitely slow decaying synapses ($\alpha \to 0$). In this case each neuron in the bump receives constant above threshold input and thus all neurons within the bump will fire with rate one. All neurons outside of the bump receive below threshold input and never fire. We suppose that a bump, $g(x,t) = q(x,t)$, exists on the domain $L = [x_1, x_2]$. This implies that $q(x,t)$ is above threshold on L and below threshold outside of L and equal to the threshold at $x = x_1$ and x_2. From (162)

$$q(x,t) = \int_{x_1}^{x_2} w(x-y)P(t-\phi(y))\mathrm{d}y, \tag{167}$$

where $P(t) = \sum_m \eta(t-m)$ is a periodic function (with period one) and $\phi(y)$ is the location dependent phase. If $w(x)$ is symmetric, we only need to consider one edge. For infinitely slow synapses $P(t) = 1$. This leads to the Amari existence condition

$$h = \int_0^{\Delta} w(y)\mathrm{d}y, \qquad \Delta = x_2 - x_1. \tag{168}$$

We note that in the Amari limit the bump solution is insensitive to the phases of the neurons. Importantly, it is possible to construct a class of bump solutions for the full continuum Lighthouse model, and thus take a step beyond the standard Amari style analysis of localised states. For the original Lighthouse model with instant phase reset whenever activity drops below threshold, an equiperiod bump is expected since neurons within the bump will fire with rate one and those outside of the bump will not fire. For the second version without the phase reset condition, phases may ride on long sub-threshold plateaus. In this case the generic solution is a spatially localised solution with an 'interior' and 'exterior' region. Within the interior, neurons fire with rate one. In the exterior, the firing rate falls off to zero as the bump edge is approached. However, the contribution from the exterior region only weakly perturbs the location of the inner edge, so that the solution in the absence of a phase reset may be regarded as a perturbation of the one with a phase reset.

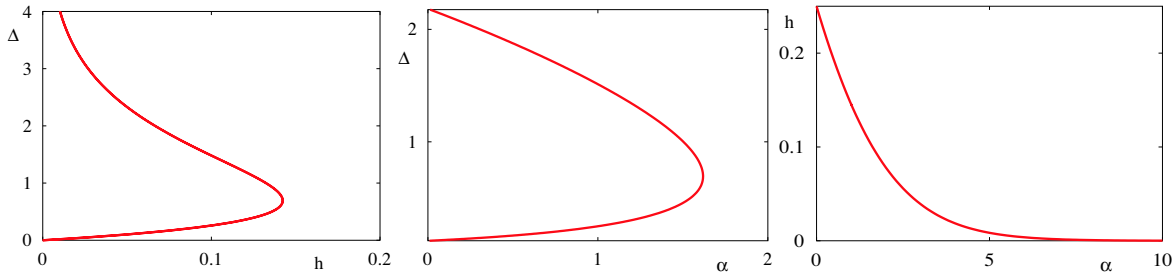

Figure 7: Left: Bump width as a function of h for the synchronous solution ($\beta = 0$) with $\alpha = 1$. Middle: Bump width as a function of α for the synchronous solution with $h = 0.1$. Right: Existence window (below the curve) for the synchronous solution in the (α, h) plane obtained by the numerical continuation of the limit point in the left hand plot. In all plots $A = a = 2$.

Here we focus on the class of (symmetric) maximally firing one-bump solutions (with firing rate unity) for the instant reset model parameterised by

$$T^m(x) = m + [\beta|x| \mod 1], \tag{169}$$

such that $q(x,t) \geq h$ for $x \in [x_1, x_2]$ for all t, and $q(x,t) < h$ otherwise. Here we take $x_1 = -\Delta/2 = -x_2$. We are free to choose such a coordinate system by translational invariance of the continuum model. In this case $q(x,t)$ is given by (167) with $\phi(y) = \beta|y|$. Introducing the Fourier transform $\widehat{P}(k) = \int_{-\infty}^{\infty} \mathrm{d}t P(t)\mathrm{e}^{-ikt}$ means that we may write (167) as

$$q(x,t) = \int_{-\infty}^{\infty} \frac{\mathrm{d}k}{2\pi} \widehat{P}(k) F(k,x) \mathrm{e}^{ikt}, \tag{170}$$

where

$$F(k,x) = \int_{x_1}^{x_2} w(x-y)\mathrm{e}^{-ik\beta|y|}\mathrm{d}y. \tag{171}$$

Note that $q(x,t)$ has period one (inherited from $P(t)$). It is also continuous if β is nonzero. For slow synapses $P(t)$ may be regarded as a constant so that $\widehat{P}(k) = 2\pi\delta(k)$. In this case (170) becomes time-independent, with $q(x,t) = F(0,x)$. Moreover, the width of the bump is independent of β and is given implicitly by $h = F(0,\Delta/2)$. This solution is identical to the one bump solution describing the time-independent localised state of the standard Amari model. In general, however, we proceed with the evaluation of (170) using the result that

$$\widehat{P}(k) = 2\pi\widehat{\eta}(k)\sum_n \delta(k - 2\pi n). \tag{172}$$

Substitution into (170) gives us the following Fourier series representation for $q(x,t)$:

$$q(x,t) = \sum_n \widehat{\eta}(2\pi n) F(2\pi n, x)\mathrm{e}^{2\pi i n t}. \tag{173}$$

To determine the width of a bump in a self-consistent fashion we must enforce the condition that at the boundaries $x = x_j$, the infimum of q (over t) must equal the threshold h. Hence, the existence condition for a bump in the continuum Lighthouse model is simply

$$\inf_t q(\Delta/2, t) = h. \tag{174}$$

The bump width Δ is then determined by

$$h = \int_0^{\Delta} w(y)\mathrm{d}y + 2\mathrm{Re}\left(\sum_{n>0} \widehat{\eta}(2\pi n) G(2\pi n)\mathrm{e}^{2\pi i n t^*}\right), \tag{175}$$

where $G(k) = F(k, \Delta/2)$. Here t^* denotes the value of t for which $q(\Delta/2, t)$ has a minimum. The value of t^* is calculated by differentiating (173) and then solving

$$0 = \mathrm{Re}\left(i\sum_{n>0} \widehat{\eta}(2\pi n) G(2\pi n) n \mathrm{e}^{2\pi i n t^*}\right), \tag{176}$$

subject to $\partial_{tt} q(\Delta/2, t)|_{t=t^*} > 0$. In some sense we may regard the second term on the right hand side of (175) as a correction to the standard Amari firing rate model description that takes into account the effects of non-slow synaptic processing.

For our choice of temporal and spatial kernels a short calculation gives $\widehat{\eta}(k) = \alpha/(\alpha + ik)$, and

$$\begin{aligned} G(k) = A\left\{\frac{\mathrm{e}^{-ik\beta\Delta/2} - \mathrm{e}^{-a\Delta/2}}{a - ik\beta} + \frac{\mathrm{e}^{-a\Delta/2} - \mathrm{e}^{-a\Delta}\mathrm{e}^{-ik\beta\Delta/2}}{a + ik\beta}\right\} \\ - \frac{\mathrm{e}^{-ik\beta\Delta/2} - \mathrm{e}^{-\Delta/2}}{1 - ik\beta} + \frac{\mathrm{e}^{-\Delta/2} - \mathrm{e}^{-\Delta}\mathrm{e}^{-ik\beta\Delta/2}}{1 + ik\beta}. \end{aligned} \tag{177}$$

In the limit $\alpha \to 0$ the β-independent shape of a bump is given explicitly by

$$q(x) = \begin{cases} W(x_1 - x, x_2 - x) & x < x_1 \\ W(0, x - x_1) + W(0, x_2 - x) & x_1 \le x \le x_2 \\ W(x - x_2, x - x_1) & x > x_2, \end{cases} \tag{178}$$

where

$$W(x_a, x_b) = \int_{x_a}^{x_b} w(y)\mathrm{d}y = \frac{A}{a}\left[\mathrm{e}^{-ax_a} - \mathrm{e}^{-ax_b}\right] - \left[\mathrm{e}^{-x_a} - \mathrm{e}^{-x_b}\right], \qquad x_b > x_a > 0, \tag{179}$$

and Δ satisfies $h = \int_0^\Delta w(y)\mathrm{d}y$. This is the classic Amari bump. When $q(x) > h$, the neuron fires with rate 1. Of the two branches of solutions to $\Delta = \Delta(h)$, the branch with largest Δ is stable for all α (see section 3.2.2). To see the effects of a non-zero choice of α in the Lighthouse model we need only to calculate remaining terms from the right hand side of (175).

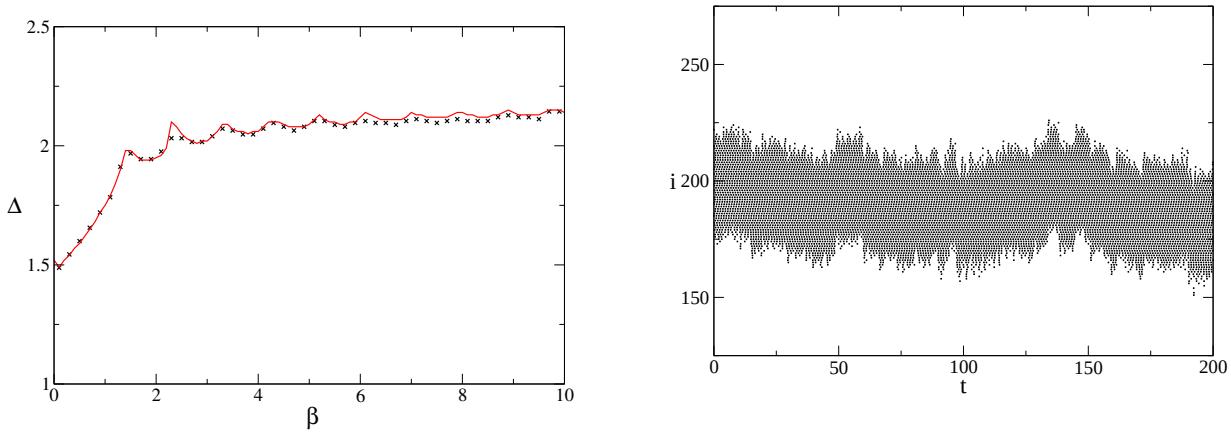

Figure 8: Left: A plot of the theoretical curve (red) for $\Delta = \Delta(\beta)$ with $h = 0.1$ and other parameters as in the left hand panel of Fig. 7. Black crosses denote results from direct numerical simulations of the Lighthouse model with instant reset. Right: Raster of a wandering bump. Parameters are $N = 400$, $h = 0.1$, $w_{ij} = 2.1\mathrm{e}^{-|i-j|/60} - 2\mathrm{e}^{-|i-j|/75}$ and $\alpha = 3.5$.

We evaluate (175) and (176) numerically to determine the pair (Δ, t^*) as a function of system parameters. An example of this is shown in Fig. 7, where for a fixed (non-zero) value of α we plot $\Delta = \Delta(h)$ for the synchronous solution ($\beta = 0$). As for the standard Amari solution we see two branches of solutions with a saddle-node bifurcation with increasing h. Moreover, taking α as the bifurcation parameter shows that such solutions cannot exist if α is chosen too large, as once again there is a saddle-node bifurcation as seen in the middle panel of Fig. 7. In the right hand panel of Fig. 7 we effectively combine the information from the other two panels into an *existence* plot, such that synchronous solutions are found below the curve shown in the (α, h) plane. In Fig. 8 we show a plot of how the solution with the largest width varies as a function of β. This theoretical curve is compared with direct numerical simulations of the instant reset Lighthouse model and found to be in excellent agreement. Moreover, simulations show that with increasing α bumps can lose stability and begin to wander, as shown in Fig. 8 (right) The wandering is reminiscent of a random walk. This implies that the position of the inner edge of a bump x will obey $\langle (x(t) - x(t-\tau))^2 \rangle = D\tau$. Simulations

suggest that $D = D(\alpha) \propto e^{k\alpha}$ [18]. One remaining challenge is to analytically determine the conditions for bump stability.

Acknowledgements

I would like to thank Ruth Smith for a careful reading of these notes.

References

[1] S Amari. Homogeneous nets of neuron-like elements. *Biological Cybernetics*, 17:211–220, 1975.

[2] S Amari. Dynamics of pattern formation in lateral-inhibition type neural fields. *Biological Cybernetics*, 27:77–87, 1977.

[3] F Apfaltrer, C Ly, and D Tranchina. Population density methods for stochastic neurons with realistic synaptic kinetics: Firing rate dynamics and fast computational methods. *Network: Computation in Neural Systems*, 17:373 – 418, 2006.

[4] R Ben-Yishai, L Bar-Or, and H Sompolinsky. Theory of orientation tuning in visual cortex. *Proceedings of the National Academy of Sciences USA*, 92:3844–3848, 1995.

[5] I Bojak and D T J Liley. Modeling the effects of anesthesia on the electroencephalogram. *Physical Review E*, 71:041902, 2005.

[6] S E Boustani and A Destexhe. A master equation formalism for macroscopic modeling of asynchronous irregular activity states. *Neural Computation*, 21:46–100, 2009.

[7] C A Brackley and M S Turner. Random fluctuations of the firing rate function in a continuum neural field model. *Physical Review E*, 75:041913, 2007.

[8] P C Bressloff. New mechanism for neural pattern formation. *Physical Review Letters*, 76:4644–4647, 1996.

[9] P C Bressloff. Traveling fronts and wave propagation failure in an inhomogeneous neural network. *Physica D*, 155:83–100, 2001.

[10] P C Bressloff. Stochastic neural field theory and the system-size expansion. *SIAM Journal on Applied Mathematics, submitted*, 2009.

[11] P C Bressloff and S Coombes. Physics of the extended neuron. *International Journal of Modern Physics B*, 11:2343–2392, 1997.

[12] P C Bressloff and S Coombes. Dynamics of strongly-coupled spiking neurons. *Neural Computation*, 12:91–129, 2000.

[13] P C Bressloff, J D Cowan, M Golubitsky, P J Thomas, and M Wiener. Geometric visual hallucinations, Euclidean symmetry and the functional architecture of striate cortex. *Philosophical Transactions of the Royal Society London B*, 40:299–330, 2001.

[14] P C Bressloff and B De Souza. Neural pattern formation in networks with dendritic structure. *Physica D*, 115:124–144, 1998.

[15] M A Buice, J D Cowan, and C C Chow. Systematic fluctuation expansion for neural network activity equations. *Neural Computation, to appear*, 22:377–426, 2010.

[16] D Cai, L Tao, M Shelley, and D W McLaughlin. An effective kinetic representation of fluctuation-driven neuronal networks with application to simple and complex cells in visual cortex. *Proceedings of the National Academy of Sciences of the United States of America*, 101:7757–7762, 2004.

[17] R D Chervin, P A Pierce, and B W Connors. Periodicity and directionality in the propagation of epileptiform discharges across neortex. *Journal of Neurophysiology*, 60:1695–1713, 1988.

[18] C C Chow and S Coombes. Existence and wandering of bumps in a spiking neural network model. *SIAM Journal on Applied Dynamical Systems*, 5:552–574, 2006.

[19] C L Colby, J R Duhamel, and M E Goldberg. Oculocentric spatial representation in parietal cortex. *Cerebral Cortex*, 5:470–481, 1995.

[20] B W Connors and Y Amitai. Generation of epileptiform discharges by local circuits in neocortex. In P A Schwartzkroin, editor, *Epilepsy: Models, Mechanisms and Concepts*, pages 388–424. Cambridge University Press, 1993.

[21] S Coombes. Waves, bumps, and patterns in neural field theories. *Biological Cybernetics*, 93:91–108, 2005.

[22] S Coombes. Large-scale neural dynamics: Simple and complex. *NeuroImage*, 52:731–739, 2010.

[23] S Coombes, C R Laing, H Schmidt, N Svanstedt, and J A Wyller. Waves in random neural media. *Discrete and Continuous Dynamical Systems Series A*, to appear, 2011.

[24] S Coombes, G J Lord, and M R Owen. Waves and bumps in neuronal networks with axo-dendritic synaptic interactions. *Physica D*, 178:219–241, 2003.

[25] S Coombes and M R Owen. Evans functions for integral neural field equations with Heaviside firing rate function. *SIAM Journal on Applied Dynamical Systems*, 34:574–600, 2004.

[26] S Coombes, H Schmidt, and I Bojak. Interface dynamics in planar neural field models. *Journal of Mathematical Neuroscience*, submitted, 2011.

[27] S Coombes, Y Timofeeva, C-M Svensson, G J Lord, K Josic, S J Cox, and C M Colbert. Branching dendrites with resonant membrane: A "sum-over-trips" approach. *Biological Cybernetics*, 97:137–149, 2007.

[28] S Coombes, N A Venkov, L Shiau, I Bojak, D T J Liley, and C R Laing. Modeling electrocortical activity through improved local approximations of integral neural field equations. *Physical Review E*, 76:051901, 2007.

[29] F L da Silva and A Van Rotterdam. *Electroencephalography: Basic principles, clinical applications and related fields*, chapter Biophysical aspects of EEG and Magnetoencephalogram generation, pages 107–126. Lippincott Williams & Wilkins, 2005.

[30] B Ermentrout. Stripes or spots? Nonlinear effects in bifurcation of reaction-diffusion equations on the square. *Proceedings of the Royal Society of London. Series A*, 434:413–417, 1991.

[31] G B Ermentrout. Neural nets as spatio-temporal pattern forming systems. *Reports on Progress in Physics*, 61:353–430, 1998.

[32] G B Ermentrout and J D Cowan. A mathematical theory of visual hallucination patterns. *Biological Cybernetics*, 34:137–150, 1979.

[33] G B Ermentrout and D Kleinfeld. Traveling electrical waves in cortex: Insights from phase dynamics and speculation on a computational role. *Neuron*, 29:33–44, 2001.

[34] G B Ermentrout and J B McLeod. Existence and uniqueness of travelling waves for a neural network. *Proceedings of the Royal Society of Edinburgh*, 123A:461–478, 1993.

[35] J Evans. Nerve axon equations: IV The stable and unstable impulse. *Indiana University Mathematics Journal*, 24:1169–1190, 1975.

[36] O Faugeras, F Grimbert, and J-J Slotine. Absolute stability and complete synchronization in a class of neural fields models. *SIAM Journal on Applied Mathematics*, 69:205–250, 2008.

[37] I Ginzburg and H Sompolinsky. Theory of correlations in stochastic neural networks. *Physical Review E*, 50:3171–3191, 1994.

[38] P S Goldman-Rakic. Cellular basis of working memory. *Neuron*, 14:477–485, 1995.

[39] D Golomb and Y Amitai. Propagating neuronal discharges in neocortical slices: Computational and experimental study. *Journal of Neurophysiology*, 78:1199–1211, 1997.

[40] H Haken. Phase locking in the lighthouse model of a neural net with several delay times. *Progress of Theoretical Physics*, 139:96–111, 2000.

[41] H Haken. Quasi-discrete dynamics of a neural net: The lighthouse model. *Discrete Dynamics in Nature and Society*, 4:187–200, 2000.

[42] H Haken. *Brain Dynamics: Synchronization and Activity Patterns in Pulse-coupled Neural Nets with Delays and Noise*. Springer-Verlag, 2002.

[43] R Hoyle. *Pattern formation: An introduction to methods*. Cambridge University Press, 2006.

[44] X Huang, W C Troy, Q Yang, H Ma, C R Laing, S J Schiff, and J Wu. Spiral waves in disinhibited mammalian neocortex. *The Journal of Neuroscience*, 24:9897–9902, 2004.

[45] V K Jirsa and H Haken. Field theory of electromagnetic brain activity. *Physical Review Letters*, 77:960–963, 1996.

[46] J A S Kelso, S L Bressler, S Buchanan, G C Deguzman, M Ding, A Fuchs, and T Holroyd. A phase-transition in human brain and behaviour. *Physics Letters A*, 169:134–144, 1992.

[47] U Kim, T Bal, and D A McCormick. Spindle waves are propagating synchronized oscillations in the ferret LGNd *in vitro*. *Journal of Neurophysiology*, 74:1301–1323, 1995.

[48] K Kishimoto and S Amari. Existence and stability of local excitations in homogeneous neural fields. *Journal of Mathematical Biology*, 7:303–318, 1979.

[49] B Kriener, T Tetzlaff, A Aertsen, M Diesmann, and S Rotter. Correlations and population dynamics in cortical networks. *Neural Computation*, 20:2185–2226, 2008. PMID: 18439141.

[50] C Laing and C C Chow. Stationary bumps in networks of spiking neurons. *Neural Computation*, 13:1473–1494, 2001.

[51] C R Laing and W C Troy. PDE methods for nonlocal models. *SIAM Journal on Applied Dynamical Systems*, 2:487–516, 2003.

[52] C R Laing, W C Troy, B Gutkin, and G B Ermentrout. Multiple bumps in a neuronal model of working memory. *SIAM Journal on Applied Mathematics*, 63:62–97, 2002.

[53] A Mazaheri and O Jensen. Rhythmic pulsing: Linking ongoing brain activity with evoked responses. *Frontiers in Human Neuroscience*, 4(0), 2010.

[54] R Miles, R D Traub, and R K S Wong. Spread of synchronous firing in longitudinal slices from the CA3 region of Hippocampus. *Journal of Neurophysiology*, 60:1481–1496, 1995.

[55] P L Nunez. The brain wave equation: a model for the EEG. *Mathematical Biosciences*, 21:279–297, 1974.

[56] D Q Nykamp and D Tranchina. A population density approach that facilitates large-scale modeling of neural networks: Extension to slow inhibitory synapses. *Neural Computation*, 13:511–546, 2001.

[57] K H Pettersen and G T Einevoll. Amplitude variability and extracellular low-pass filtering of neuronal spikes. *Biophysical Journal*, 94:784–802, 2008.

[58] D J Pinto and G B Ermentrout. Spatially structured activity in synaptically coupled neuronal networks: I. Travelling fronts and pulses. *SIAM Journal on Applied Mathematics*, 62:206–225, 2001.

[59] P A Robinson, C J Rennie, J J Wright, H Bahramali, E Gordon, and D l Rowe. Prediction of electroencephalographic spectra from neurophysiology. *Physical Review E*, 63:021903, 2001.

[60] B Sandstede. *Handbook of Dynamical Systems II*, chapter Stability of travelling waves, pages 983–1055. Elsevier, 2002.

[61] H Schmidt, A Hutt, and L Schimansky-Geier. Wave fronts in inhomogeneous neural field models. *Physica D*, 238:1101–1112, 2009.

[62] I Segev, J Rinzel, and G M Shepherd, editors. *The theoretical foundations of dendritic function: selected papers of Wilfrid Rall with commentaries*. MIT Press, 1995.

[63] H Soula and C C Chow. Stochastic dynamics of a finite-size spiking neural network. *Neural Computation*, 19:3262–3292, 2007.

[64] M Steriade, E G Jones, and R R Línas. *Thalamic Oscillations and Signalling*. Wiley, New York, 1990.

[65] M L Steyn-Ross, D A Steyn-Ross, J W Sleigh, and D T J Liley. Theoretical electroencephalogram stationary spectrum for a white-noise-driven cortex: Evidence for a general anesthetic-induced phase transition. *Physical Review E*, 60:7299–7311, 1999.

[66] P Tass. Cortical pattern formation during visual hallucinations. *Journal of Biological Physics*, 21:177–210, 1995.

[67] N A Venkov, S Coombes, and P C Matthews. Dynamic instabilities in scalar neural field equations with space-dependent delays. *Physica D*, 232:1–15, 2007.

[68] H R Wilson and J D Cowan. Excitatory and inhibitory interactions in localized populations of model neurons. *Biophysical Journal*, 12:1–24, 1972.

[69] H R Wilson and J D Cowan. A mathematical theory of the functional dynamics of cortical and thalamic nervous tissue. *Kybernetik*, 13:55–80, 1973.

[70] J Y Wu, L Guan, and Y Tsau. Propagating activation during oscillations and evoked responses in neocortical slices. *Journal of Neuroscience*, 19:5005–5015, 1999.

[71] K Zhang. Representation of spatial orientation by the intrinsic dynamics of the head-direction cell ensemble: A theory. *Journal of Neuroscience*, 16:2112–2126, 1996.